**ISTANBUL TECHNICAL UNIVERSITY ★ GRADUATE SCHOOL OF SCIENCE ENGINEERING AND TECHNOLOGY**

# HYDRODYNAMIC ANALYSIS OF AN UNDERWATER GLIDER

**M.Sc. THESIS**

**Mehmet Ozan ŞERİFOĞLU**

**Department of Shipbuilding and Ocean Engineering**

**Shipbuilding and Ocean Engineering Programme**

**DECEMBER 2018**

**ISTANBUL TECHNICAL UNIVERSITY ★ GRADUATE SCHOOL OF SCIENCE ENGINEERING AND TECHNOLOGY**

# HYDRODYNAMIC ANALYSIS OF AN UNDERWATER GLIDER

**M.Sc. THESIS**

**Mehmet Ozan ŞERİFOĞLU**
**(508151114)**

**Department of  Shipbuilding and Ocean Engineering**

**Shipbuilding and Ocean Engineering Programme**

**Thesis Advisor: Assist. Prof. Dr. Bilge TUTAK**

**DECEMBER 2018**

**ISTANBUL TEKNİK ÜNİVERSİTESİ ★ FEN BİLİMLERİ ENSTİTÜSÜ**

# BİR SUALTI PLANÖRÜNÜN HİDRODİNAMİK ANALİZİ

**YÜKSEK LİSANS TEZİ**

**Mehmet Ozan ŞERİFOĞLU**
**508151114**

**Gemi ve Deniz Teknolojisi Mühendisliği Anabilim Dalı**

**Gemi ve Deniz Teknolojisi Mühendisliği Programı**

**Tez Danışmanı: Dr. Öğr. Üyesi Bilge TUTAK**

**ARALIK 2018**

Mehmet Ozan ŞERİFOĞLU, a M.Sc. student of İTU Graduate School of Science Engineering and Technology student ID 508151114, successfully defended the thesis entitled "HYDRODYNAMIC ANALYSIS OF AN UNDERWATER GLIDER", which he prepared after fulfilling the requirements specified in the associated legislations, before the jury whose signatures are below.

| | | |
|---|---|---|
| **Thesis Advisor :** | **Assist. Prof. Dr. Bilge TUTAK**<br>İstanbul Technical University | .............................. |
| **Jury Members :** | **Assist. Prof. Dr. Serdar A. KÖROĞLU**<br>Istanbul Technical University | ............................. |
| | **Prof. Dr. Cem GAZİOĞLU**<br>Istanbul University | .............................. |

**Date of Submission : 16 November 2018**
**Date of Defense : 10 December 2018**

***To my family and friends,***

## FOREWORD

I would like to thank many people who helped me in one way or another during the span of this research. Unfortunately, I can only name a few of them here. First, I would like show my gratitude to my thesis supervisor Assist. Prof. Dr. Bilge Tutak for sharing his knowledge and insight with me not just for this work but also for other times I needed. I would like to thank my business partner Turgay Hızarcı for all the patience he showed me while I am working on this project and not being able to help him much.

I would especially like to acknowledge the help of Gürbüz Bilici. He helped me to shape foundation of this research, pointed me to right sources to increase my knowledge on the subject and answered my questions tirelessly.

I also would like to thank my parents for supporting me and to Tuğçe Ecem Tüfek for being with me all the time through this period. She showed me a lot of patience, understanding and carried me through psychologically.

This research has been funded by ITU BAP (Scientific Research Projects) Department as a Master's Degree Project.

I hope this study could be useful to someone on their own research.

November 2018

Mehmet Ozan ŞERİFOĞLU
Marine Engineer

**TABLE OF CONTENTS**

**Page**

## ABBREVIATIONS

**ADCP** : Acoustic Doppler Current Profiler
**ASV** : Autonomous Surface Vehicle
**AUG** : Autonomous Underwater Glider
**AUV** : Autonomous Underwater Vehicle
**CFD** : Computational Fluid Dynamics
**CTD** : Conductivity, Temperature, Depth
**DO** : Dissolved Oxygen
**GAMG** : Generalized Geometric-Algebraic Multi-Grid
**GPS** : Global Positioning System
**OSUG** : Open Source Underwater Glider
**PAR** : Photosynthetically Active Radiation
**RANS** : Reynolds Averaged Navier Stokes
**RF** : Radio Frequency
**RNG** : Re-Normalization Group
**ROV** : Remotely Operated Vehicle
**SIMPLE** : Semi-Implicit Method for Pressure Linked Equations
**SIMPLEC** : Semi-Implicit Method for Pressure Linked Equations-Consistent
**SST** : Shear Stress Transport
**UMS** : Unmanned Maritime Systems
**USV** : Unmanned Surface Vehicle
**UUV** : Unmanned Underwater Vehicle

**SYMBOLS**

| | |
|---|---|
| **ρ** | : Density |
| **L** | : Watertight length |
| $\mathbf{L_{oa}}$ | : Overall length |
| **D** | : Diameter |
| **k** | : Turbulence kinetic energy |
| **ω** | : Specific rate of dissipation |
| **n** | : Myring coefficient of nose section |
| **θ** | : Myring coefficient of back section |
| **U** | : Velocity |
| **p** | : Pressure |
| **Re** | : Reynolds Number |
| $\mathbf{C_D}$ | : Drag coefficient |
| $\mathbf{C_L}$ | : Lift coefficient |
| $\mathbf{C_P}$ | : Pressure coefficient |
| $\mathbf{y^+}$ | : Dimensionless wall distance |
| **V** | : Volume |

## LIST OF TABLES

**LIST OF FIGURES**

**Page**

**HYDRODYNAMIC ANALYSIS OF AN UNDERWATER GLIDER**

## SUMMARY

Autonomous underwater gliders are underwater vehicles that can travel underwater by changing their buoyancy and center of gravity. This movement mechanism grant underwater gliders the longest mission endurance among all autonomous underwater vehicles with 6 to 12 months of active time. In this period, these vehicles can collect various kinds of ocean data over thousands of kilometers in range and transfer that data to a control center over satellite connection. The endurance, range of operation and variety of the collectable data makes underwater gliders one of the best tools for ocean observation.

In this study, drag force on the axisymmetric torpedo shaped glider hulls are analyzed. Dimensions of tested forms are chosen by considering commercial and academic gliders. From there, basis dimensions for length and diameter are selected as 1.50m and 0.20m respectively. Thirteen different forms are generated for analyses. The forms include; 4 constant diameter forms with changing length (0.20m diameter with 0.50, 1.00, 2.00, 2.50 meter lengths), 5 constant length forms with changing diameter (1.5m length with 0.12, 0.16, 0.20, 0.24, 0.28m diameters) and 4 extra forms for comparison of flow separation of the forms with large diameter. Shape of the nose and back sections are chosen using Myring equations with length 0.20m nose and 0.30m back section. Nose and back sections are kept constant for all forms. The forms are analyzed in 4 different velocities (0.3, 0.6, 0.9, 1.2 m/s) and 6 different angles of attack (0, 2, 4, 6, 8, 10°) for a total of 312 analyses using the open source CFD software OpenFOAM.

The results show that volume increase effects gliders more and more as angle of attack and glider velocity increases. However for glider with velocities ranging from 0.3 to 0.6 m/s the increase in the volume does not contribute drag force as much. Moreover it is important to do nose and back sections analyses to determine the dimensions of the nose and back sections because of the increase in separation with increasing angle of attack and velocity.

# BİR SUALTI PLANÖRÜNÜN HİDRODİNAMİK ANALİZİ


## ÖZET

İnsansız Deniz Araçları, sağladıkları avantajlar ile tüm dünyada askeri ve bilimsel otoritelerin en çok tercih ettiği deniz araştırma sistemleri olma yolunda hızla ilerlemektedir. Bu araçlar farklı görevler için özelleşerek birçok alt kategoriye ayrılmıştır. İnsansız Deniz Araçları, ana olarak İnsansız Yüzey Araçları ve İnsansız Sualtı Araçları olarak iki kategoriye ayrılabilir. İnsansız yüzey araçları olarak Otonom Yüzey Aracı ve Dalga Planörü sayılabilirken, insansız sualtı araçları da Kumanda Kontrollü Sualtı Aracı, Otonom Sualtı Aracı ve Otonom Sualtı Planörü olarak alt gruplara ayrılabilirler.

Aslen bir insansız bir sualtı aracı olan Otonom Sualtı Planörleri sahip oldukları yetenekler ile kendi kategorilerini kazanmışlardır. Bu araçların en büyük özelliği araç ağırlığı, ağırlık merkezinin yeri ve araç hacmi gibi parametreleri değiştirerek su altında bilinçli bir batma-çıkma döngüsünü izleyebilmeleri ve bu esnada kanatları vasıtası ile ürettikleri kaldırma kuvvetini kullanarak ileri yönde hareket edebilmeleridir. Pervane ya da benzeri bir itki sistemi olmaksızın sağlanan bu hareket çok yüksek bir enerji verimi sağlamakta ve sualtı planörlerinin 6 ay ile 1 sene arası uzun süreler sualtında herhangi bir insan müdahalesi olmaksızın çalışabilmesini imkân vermektedir. Sualtı planörleri üzerlerinde taşıdıkları CTD, ADCP, DO, PAR vb. sensörler ile periyodik olarak sualtında veri toplayabilmekte ve bu verileri yüzeyde kurulan uydu bağlantısı yoluyla bir kontrol merkezine aktarabilmektedir. Sualtı planörleri itki sisteminden yoksun olduklarından dolayı diğer insansız sualtı araçlarına göre düşük mevki hassasiyetine sahiptirler. Sualtından kontrol merkezlerine kablosuz bir bağlantı sağlayabilecek kapasitede bir sistem olmadığında, bu araçlar henüz yüzeydeyken görev bilgilerini ve gidilmesi gereken koordinatları kontrol merkezinden alır. Daha sonra, bir sonraki yüzeye çıkış zamanına kadar aracın sualtındaki hareketleri ivmeölçer, elektronik pusula, basınç sensörleri ve altimetre sensörleri yardımlarıyla hesaplanarak tahmin edilmeye çalışılır. Araç, her yüzeye çıktığında Küresel Konumlama Sistemi üzerinden veri alarak sualtındaki tahminlerden kaynaklı oluşan hataları sıfırlar ve rutin seyrine geri döner.

Sualtı planörleri aylarca süren görev süreleri boyunca oldukça geniş çapta bir bölgeyi tarayabilirler ve 10000km gibi büyük mesafelere ulaşabilirler. Bu ve daha yüksek menzillere ancak hidrodinamik olarak iyi optimize edilmiş gövde yapılarıyla ulaşılabilmektedir. Sualtı planörlerinin toplam dirençlerinin büyük bir bölümü planörün gövdesi tarafından oluşturulmaktadır. Bu nedenle, iyi tasarlanmış bir gövde yapısı aracın hidrodinamik sürtünme performansını iyileştirerek her bir dalış ve çıkışta daha uzun mesafeler kat edebilmesi sağlayabilir. Bu şekilde kazanılan enerji, bir görev süresi boyunca düşünüldüğünde, aracın menzilini arttırabilir, belirli bir görevin daha kısa sürede bitmesini sağlayabilir, araca daha fazla sensör takmaya yetecek bir enerji bütçesi oluşturabilir ya da var olan sensör paketlerinin veri alma frekanslarında bir artış oluşmasını sağlayabilir. Bunlar gibi iyileştirmelerin sağlanabilmesi için hidrodinamik optimizasyonun sağlanması gerekmektedir. Bir sualtı planöründe,

sürtünme kuvvetinde iyileştirme sağlayabilmek için aracın çap ve boy gibi ana parametrelerinin küçültülmesi oldukça basit ve yeterli bir çözüm sunmaktadır. Ancak bu araçların deplasman hacmini oluşturan iç hacimleri, boyutların küçültülmesi konusunda sınırlayıcı faktörü oluşturmaktadır. Normal şartlarda çapta ya da boyda yapılacak küçültmeler, hali hazırda sıkışık olan iç yapının daha da sıkışarak bir takım sistemleri barındıramayacak duruma gelmesine ya da daha da önemlisi, sualtı planörlerinde ana güç kaynağı olan ve iç hacimde büyük bir paya sahip olan, batarya sisteminden eksiltme yapılmasını zorunlu kılabilir. Buradan anlaşılacağı üzere, araç üzerinde yapılabilecek hidrodinamik iyileştirmeler ancak, aracın aktif çalışma süresi üzerinde doğrudan etki sahibi olabilecek araç iç hacmi ve aracın temel boyutları arasındaki doğru oranların saptanması ile mümkün olabilmektedir. Bunların yanında sualtı planörlerinin modüler bir şekilde kullanılabilmeleri, yani aracın görevden göreve ihtiyacı olabilecek sensör paketleri, ek pil üniteleri ve ek taşıma kapasitesi sağlayacak gövde parçalarının görev bazında değiştirilebilmesi de aracın boyutlarında, üretim sonrasında dahi önemli değişiklikler olabileceğini göstermektedir. Tüm bunlar göz önüne alındığında, bir tasarımcının, yeni bir tasarıma başlarken, araç iç hacmi ve temel boyutlar arası dengeyi sağlayabilmesi ve modüler bir kullanım senaryosunda oluşabilecek yeni durumları da göz önünde bulundurabilmesi adına, temel boyut değerlerindeki değişime bağlı hidrodinamik sürtünme performansı değişimini görebilmesi gerekmektedir. Bu çalışmada, bu değişimin gösterilebilmesi için aracın boy ve çap parametrelerindeki değişimin iç hacme ve sürtünme kuvvetine etkileri gözlemlenmiştir. Gözlemler için avantajlarından dolayı sualtı planörleri için en yaygın gövde şekli olan, torpido stili gövde seçilmiştir ve gözlemler iki temel grup üzerinde yapılmıştır. Birinci grup çapı sabit tutularak araç su geçirmez boyunun değiştirildiği, ikinci grup ise boyun sabit tutularak çap değişimi yapıldığı senaryolardır. Bunlar yapılırken baş ve kıç formları, tüm geometrilerde sabit ve aynı uzunlukta kabul edilmiş ve genel olarak kabul görmüş parametreler üzerinden Myring denklemleriyle oluşturmuştur. Burada ikinci grupta çapın sabit boyda artması durumunda kıç bölgesinde yaşanabilecek ayrılmanın getirebileceği direnç farkının da gözlemlenebilmesi için aracın kıç bölgesindeki narinliğin korunduğu üçüncü bir grup oluşturulmuştur. Bu grupta çap değişimi ile beraber baş ve kıç boyları da oranlanarak değiştirilmiştir. Bu üç grubun oluşturulabilmesi için temel boy ve çap değeri ticari ve akademik sualtı planörleri incelenerek 1.50m'ye 0.20m olacak şekilde seçilmiş, boy ve çap değişimleri bu boyutlar üzerinde gerçekleştirilmiştir.

Sürtünme kuvveti analizlerinde açık kaynak kodlu bir Hesaplamalı Akışkanlar Dinamiği programı olan OpenFOAM programı kullanılmıştır. Hesaplamalar aracın tüm durumlarını gösterebilmesi adına 0.3, 0.6, 0.9 ve 1.2 m/s hızlar için ve 0, 2, 4, 6, 8, 10° atak açılarında gerçekleştirilmiştir. Toplamda 13 adet gövde 4 farklı hız ve 6 farklı atak açısı değeri kullanılarak 312 adet analiz yapılmıştır. Analizlerde, literatürde sualtı planörleri için da kabul görmüş olan tam türbülanslı akım varsayımı yapılmış ve türbülans modeli olarak RANS, *k-ω SST* modeli seçilmiştir. Düşük Reynolds durumlarında daha iyi sonuç alabilmek için $y^+$ değeri tüm analizlerde 0 ile 1 arasında tutulacak şekilde bir ağ örgüsü kullanılmıştır. Analizlerde zamandan bağımsızlık varsayımı yapılmış ve OpenFOAM'da bulunan *simpleFoam* çözücüsü kullanılmıştır. Çözüm için gerekli başlangıç koşulları, *potentialFoam* potansiyel akış çözümü kullanılarak belirlenmiştir. Seçilen HAD parametrelerinin uygunluğunun kesinleştrilmesi adına bilindik bir form olan DARPA Suboff takıntısız formu üzerinde analizler yapılmış ve sonuçlar deney değerleriyle karşılaştırılarak uygun bulunmuştur. Çalışmalarda doğru ağ örgüsünün kullanılabilmesi için temel boy ve çap değerleri kullanılarak oluşturulan model üzerine ağdan bağımsızlık analizi yapılmıştır. Bu analiz sonucunda, tüm analizlerde kullanılacak olan ağ örgüsü, simetri nedeniyle yarım gövde üzerinde 1.2M civarı hücre olacak şekilde seçilmiştir.

Çıkan sonuçlara göre hacim artışı yüksek atak açıları ve hızlar için daha çok olmak üzere sürtünme kuvvetini etkilemektedir. Ancak bakıldığında 0.3 ve 0.6 m/s hızları civarındaki hızlarda çok yüksek artışlar yaşanmamaktadır. Bu bağlamda, düşük hızlarda çalışan planörlerdeki hacim artışında hidrodinamik sürtünme kuvveti olarak çok etkilenmeyecektir. Bu da, modüler özelikte kullanılmak üzere tasarlanan bir sualtı planörü için önemli bir girdi oluşturmaktadır.

# 1. INTRODUCTION

Unmanned Marine Systems (UMS) are becoming more and more popular as they greatly satisfy different needs of various users from military to scientists and from the industry in general. They are quite versatile as they can be programmed for numerous different usage scenarios both for underwater and surface missions. These systems can be divided into two main categories as Unmanned Underwater Vehicles (UUV) and Unmanned Surface Vehicles (USV). USV is a recently developing category with two subclasses as Autonomous Surface Vehicles (ASV) and Wave Gliders while UUV is an established class with three main subclasses of Autonomous Underwater Vehicles (AUV), Remotely Operated Vehicles (ROV) and Autonomous Underwater Gliders (AUG) each with different use case scenarios. This classification can be seen in Figure 1.1 below.

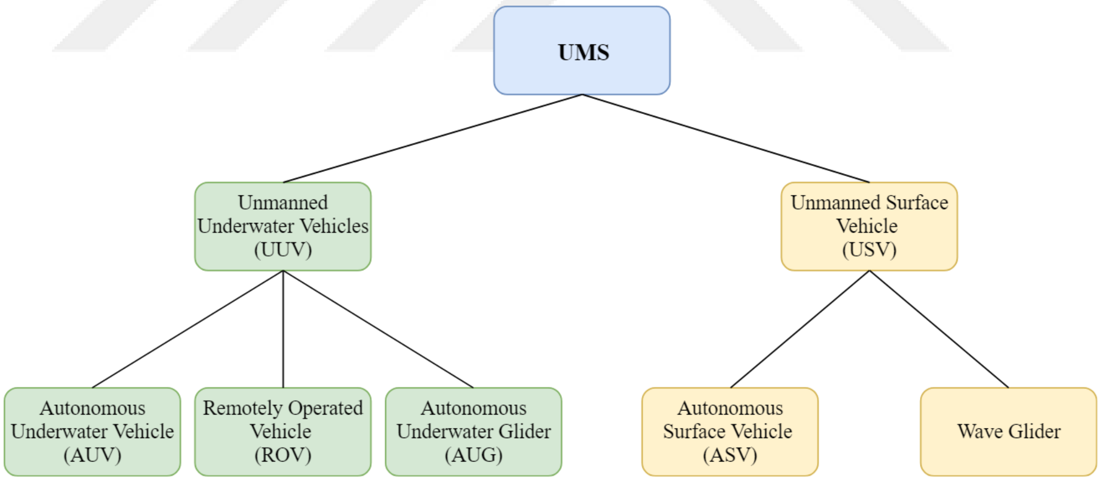


**Figure 1.1 :** Subclasses of UMS Market.

AUG is mostly a subclass of AUV but with its unique capabilities earned itself its own category. In the Figure 1.2 below, an example of an AUG can be seen. AUG are vehicles that can change their buoyancy, center of gravity and weight depending on the specific design. They can maintain a gliding motion underwater using its wings and doing a pattern of sawtooth while moving forward as seen from the illustration in Figure 1.3. As they do not have any high energy consuming propulsion mechanisms they can tolerate mission lengths changing from 6 to 12 months. In that period, they can collect several different kinds of data using different sensory equipment and transfer that data to a control center over radio frequency or satellite connection. This great endurance gives AUGs the ability to sweep a large amount of water volume over a wide range, enabling its users to create a profile of the water volume.

**Figure 1.2 :** Underwater glider (“WHOI Underwater Glider Operations”, n.d.).

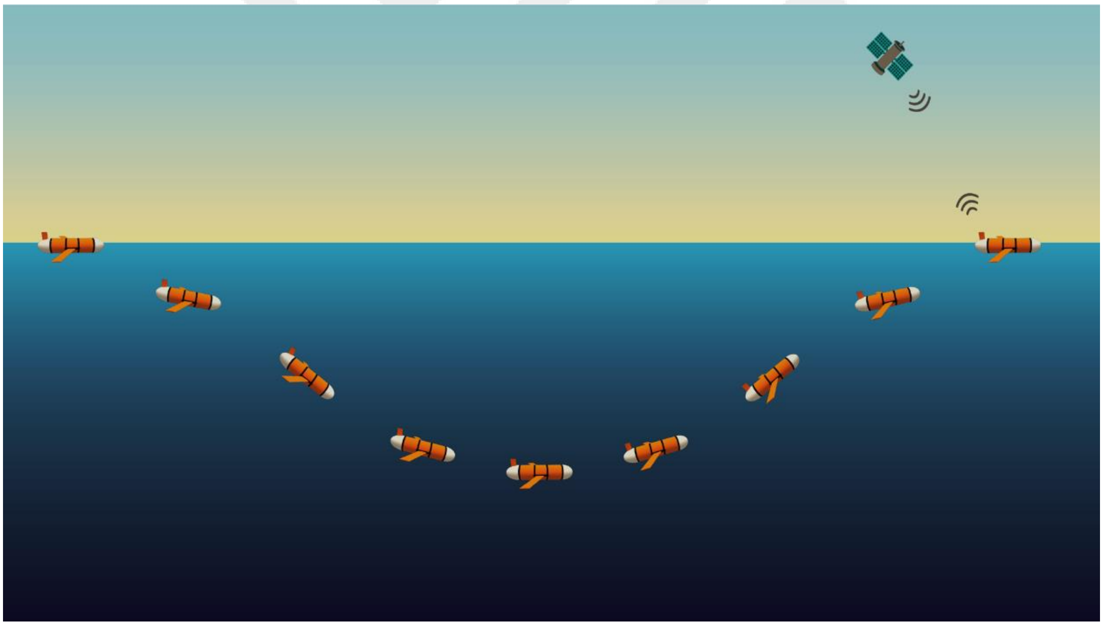

**Figure 1.3 :** Sawtooth pattern of an underwater glider.

## 1.1 Buoyancy Driven Underwater Gliders

Stommel imagined on ocean observation system formed by neutrally-buoyant floats that can change weight to move vertically and can move straight by gliding on wings, before first autonomy floats were operational (Davis, Eriksen, & Jones, 2002). After this, first AUVs and later underwater gliders as a subclass of AUVs became reality. Today, underwater gliders with several different designs are being produced.

However, the ones that are called as legacy gliders are Seaglider, Spray and Slocum (Singh, Bhattacharyya, & Idichandy, 2017). If the subject is underwater gliders these three vehicles come directly into the mind.

When an underwater glider is inspected in detail, there are different parts that control navigation and scientific actions of the glider. Main sections on a glider can be seen in the Figure 1.4. Navigation system of the glider consists of buoyancy and center of gravity control subsystems. Buoyancy pump, internal tank and external bladder composes of the buoyancy control system, while center of gravity control system includes a heavy, moving weight and an actuator that controls its movement. Buoyancy pump takes a low density fluid (can be a hydraulic liquid with a density around 900 $kg/m^3$ and/or a gas) from internal reservoir and pumps it to the external bladder outside of the water-tight volume to increase total buoyancy of the vehicle and causing vehicle to rise. The opposite of this action reduces total buoyancy of the vehicle resulting in a dive. Upward and downward motions occur as a result of this buoyancy change, but to gain forward motion glider requires an appropriate pair of wings and an appropriate angle of attack. Angle of attack adjustments are done by changing the pitch angle of the glider. Generally, it is done by displacing a heavy weight inside the vehicle with the help of an actuator. As the inside part of a glider is a very confined space, commercial gliders use what is already inside of the hull to change the center of gravity. The heaviest movable weight inside of a glider's hull is the battery packs. Total weight of battery inside of a glider can reach up to 30% to the glider's total weight (T. Hızarcı, personal communication, September 9, 2018). Therefore, weight of the battery packs is generally used for changing pitch angle of the glider. Battery packs can also be used for changing the heading of the vehicle by rolling. Rolling motion of an asymmetric battery pack grants both rolling and turning motion to the glider. Turning the vehicle can also be done by using conventional rudder setup.

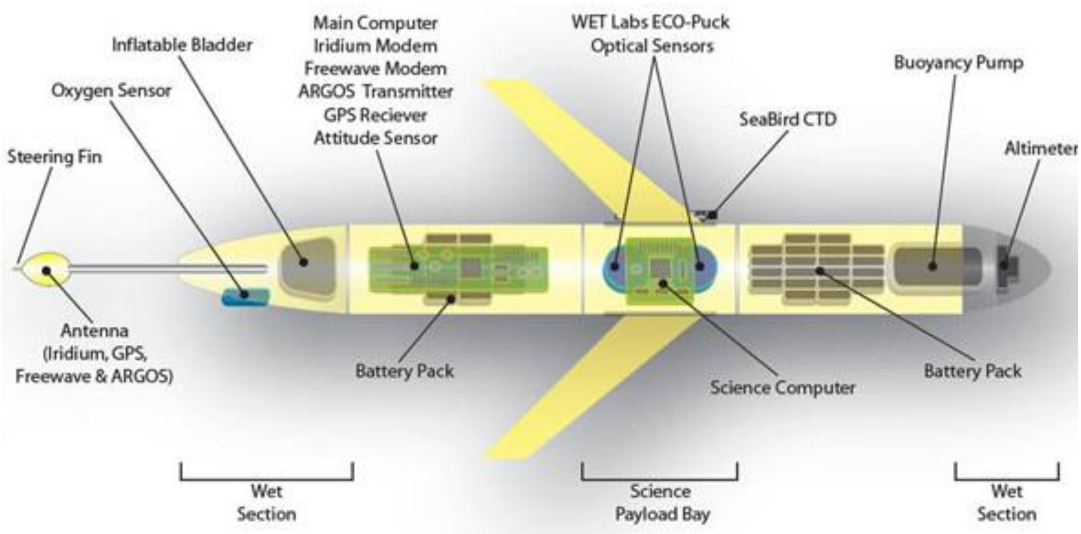


**Figure 1.4 :** Parts of an underwater glider (Harada, 2010).

Navigation control of the glider is done using variety of sensor such as pressure sensors, inertial measurement units, gyroscopes, magnetometers and altimeters. Inertial measurement unit and gyroscopes give information on physical orientation of the glider such as pitch and roll angles and help calculating velocity of the vehicle as well as the distance covered. Magnetometers provide information on heading of the vehicle. It is one of the most important sensors on the navigation, therefore should be calibrated carefully. A subsea altimeter is used to determine elevation of the vehicle from the seabed (Kongsberg Maritime, n.d.). Elevation information can change depending on the seabed material (rock, sand or mud) so there should be a general understanding of the properties of mission location. All the information generated by these sensors is combined at the main board (motherboard) of the vehicle to be processed. As there is no active propulsion system like propellers, navigational accuracy of the gliders is not very high. Generally speaking, gliders can stay in a football field sized area (around 100x70 meters) around their assigned coordinates (Shapiro, 2017). Because of this, once in a while the vehicle surfaces and receives a GPS fix to reduce the error accumulation and sends its coordinate to the user.

Underwater gliders can house several different scientific sensors. They can hold multiple sensors at once so they are able to provide the scientists with many data types on every mission. Hızarcı states that ADCP (Acoustic Doppler Current Profiler), PAR (Photosynthetically Active Radiation), CTD (Conductivity-Temperature-Depth), DO (Dissolved oxygen) and fluorometers are the sensors that can be used in underwater gliders (2015). Furthermore, other advanced sensors such as side scan sonars, nitrate sensors and samplers are being implemented to underwater gliders. An Acoustic Doppler Current Profiler (ADCP) uses Doppler shift principle to measure 3D velocity profile in the water volume (Kostaschuk, Best, Villard, Peakall, & Franklin, 2005). On a glider it helps extracting velocities in a water column from surface to the seabed. Photosynthetically active radiation (PAR) sensor measures suitable radiation levels for photosynthesis. CTD is the main sensory equipment for every underwater glider, as it supplies information on salinity and temperature of water by measuring conductivity, temperature and pressure data. Dissolved oxygen (DO) sensor measures levels of dissolved oxygen in water.

Data gathered by the sensors are periodically transferred to the control centers while the glider is on the sea surface. As a result of this, the navigation and the scientific data can be processed immediately without the need of waiting the end of the mission, also ensuring the safety of the data (in case of instrument loss). Common communication types available to an underwater glider are Iridium modem, ARGOS transmitter, GPS receiver, and RF transmitter. Radio frequency transmitters are commonly used for short range transfer of small data parts. GPS receivers help determine the exact location of the glider in between dives. ARGOS and Iridium satellite connections are used as main data transfer system for underwater gliders in general.

In the following years underwater glider usage for scientific and military purposes is expected to increase due to unique properties of these vehicles. Deep water gliders have potential to reach depths up to 6000 meters and 10000km range parallel to sea level with a mission span of 1 year ("The Next Frontier in Ocean Exploration", n.d.). While 10000km is a very impressive range for an underwater vehicle, the efficiency can still be improved via hydrodynamic optimization. Eriksen et al. (2001) states that ocean stratification, hydrodynamic drag and compressibility difference between the glider and seawater are the sources of energy expenditure for a buoyancy driven AUV. He also indicates even at the slower speeds, drag is the most significant of these expenditures. By reducing hydrodynamic drag force on a glider we can enable them to glide for longer distances on each dive. Over the course of the mission, this may increase the range of the mission, reduce time taken for a specific mission, create enough energy budget for more sensors on board or give a chance of increasing sampling rate of the existing sensors. Thus, optimizing drag force acting on a glider body creates many opportunities for a better usability and efficiency.

Several external features of an underwater glider contribute to drag creation. The main contributors are; vehicle hull, wings, rudder, antenna and sensory equipment outside of hull. The main drag generator is the hull (Singh et al., 2017). Hence, lowering dimensions of the hull may greatly decrease the drag force acting on the glider. On the other hand, increasing the dimensions may provide enough space for more batteries or more sensor. What is more, internal space of a glider is already so confined that almost every little space is occupied by a mechanical or electronic hardware as can be seen in the Figure 1.5. Therefore, there are some limiting factors for minimum length and diameter of the hull.

**Figure 1.5 :** Inside of an underwater glider (Fratantoni, 2008).

All in all, hydrodynamic design of an underwater glider should contain a good balance between the drag force acting on the hull and internal volume of the watertight section. Although right dimension may change depending on the specific mission requirements, it is a good idea to comprehend what is sacrificed well.

## 1.2 Existing Underwater Glider Hull Designs

There are several different possibilities for hull design of a glider. Most of these designs can be gathered in four subsections and those are torpedo hull form, teardrop hull form, flying wing glider form and experimental/newly emerging hull forms. Each of these types have their advantages and disadvantages for different cases.

Torpedo body shapes have a cylindrical middle body with appropriate nose and back sections. Nose and tail sections are generally wet sections. They house a number of sensors and parts of buoyancy mechanism. Nose and back sections create a hydrodynamic fairing while protecting the sensors inside. Main advantages of torpedo shaped bodies are ease of production and low manufacturing cost. They are also easier to design for high-pressure scenarios. They are also the most used ones for commercial applications. Torpedo shaped body of Slocum Glider can be seen in the Figure 1.6 below.


**Figure 1.6 :** Torpedo shaped Slocum Glider ("Teledyne Webb Research Announces Slocum Glider Service and Repair Facility in UK", 2013).

Teardrop hull (laminar body) forms focus on staying in the laminar flow region by delaying transition to turbulent flow over the hull. Its aim is not to disturb the flow as long as possible by use of a small nose cross section and a gradual increase in diameter through the back. This type of body has substantial advantage in the hull drag. Hull of Seaglider is a well-known example for this type of hull shape as seen in the Figure 1.7. Laminar flow body of Seaglider allows for a drag resistance that increases with $U^{3/2}$ rather than $U^2$ relation that can be found on gliders Slocum and Spray (Rudnick el al., 2004). However, internal space it has, is a lot less handy than torpedo shaped hulls and their production is both harder and more expensive.

**Figure 1.7 :** Seaglider with its laminar flow body (Jones, n.d.).

Flying wing glider hull as seen in the Figure 1.8, is a big wing shaped fairing. Flying wing hulls try to increase total Lift/Drag ratio of the glider by increasing contribution of the hull section to the total lift of the vehicle. In a published design study, it is stated that the designed flying wing glider has reached a L/D ratio of 13.8 which is higher than the L/D ratio of 5 of legacy gliders (Wang, Li, Wang, & Wang, 2015). This is a significant increase in L/D ratio. This way flying wing gliders can supply a very low gliding angle without losing horizontal velocity resulting in longer dive sections and less directional change. However, to resolve the structure of the ocean, glide angles should be lower than ocean property gradient, therefore the glide slopes smaller than 1:5 are meaningless (Eriksen et al., 2001). For this reason, it may be undesirable for a glider to have very low gliding slopes in most missions. Additionally, shape of the hull makes internal design of the hull harder and internal volume may not provide enough space for the parts. On the other hand, rather than examining ocean data, missions like observing marine mammals would benefit from a high lift to drag ratio (Wang et al., 2015). Therefore, flying wing glider hull can be beneficial in those types of missions.

**Figure 1.8 :** XRay Flying Wing Glider (Hildebrand, Wiggins & D'Spain, n.d.).

Newly emerging glider shapes consist of torpedo-laminar hybrid hulls, hulls inspired from marine animals, disk shaped vehicles and so on. These hull types are generally designed as an answer to a specific need, but they are not wide spread much as other types. They may require further studies to make into standardized forms. Figure 1.9 below show an example of a disk shaped glider concept.

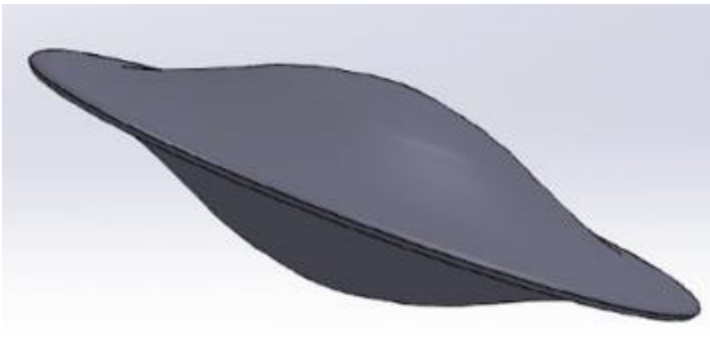

**Figure 1.9 :** Visualization of a disk shaped glider (Yu, Wang, Zhou, & Shen, 2018).

All of the glider hull forms listed above can also be arranged in modular structure meaning different groups of equipment can be separated into different modules. Modular form has advantages such as easy swapping of sensory equipment for a different mission, fast battery changing and easier glider maintenance in general. However, modular structure may sacrifice robustness of the vehicle. Using several pressure hull modules may create an opening in the water tightness of the vehicle in case of incorrect handling and may result in loss of the vehicle. Even though this is a serious drawback many of the commercial gliders are built modular to a degree. In Figure 1.10 a glider with modular nose section can be seen.

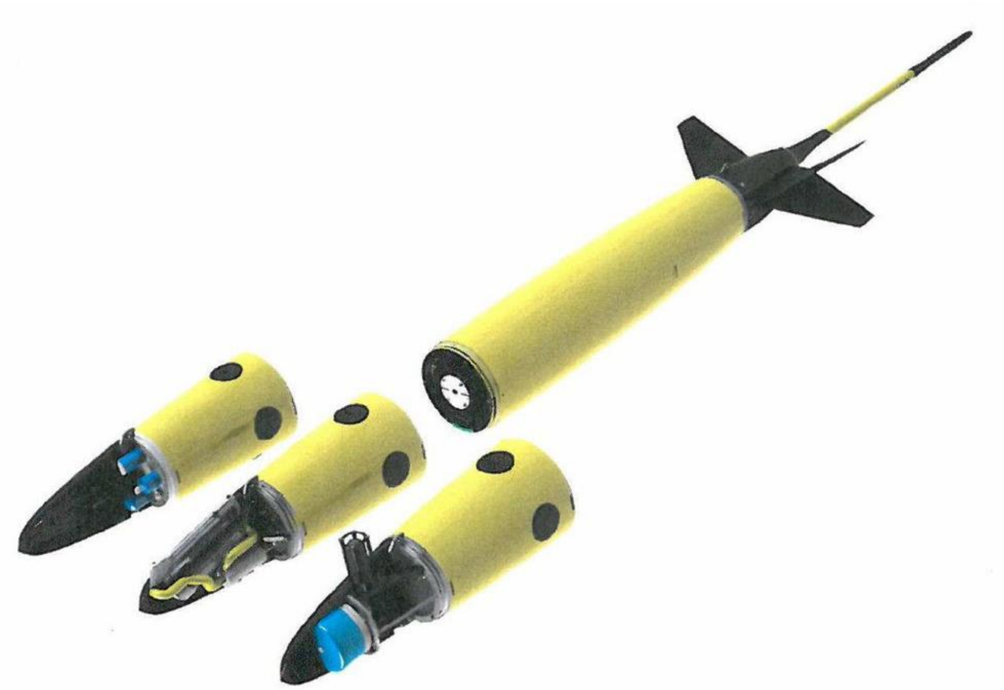

**Figure 1.10 :** A glider with modular science payload section (Szondy, 2015).

There are important gliders designed for commercial or academic purposes. Each of them have different shapes, dimensions and mission characteristics. More compact and affordable glider designs are emerging with time. In the Table 1.1 below important gliders and their respective features can be seen as a summary.

**Table 1.1 :** Dimension and velocity information of various underwater gliders.

| Name of Glider | Length (Hull - m) | Diameter (Largest - m) | Wing Span (m) | Velocity (Average - m/s) | Status |
|---|---|---|---|---|---|
| Spray | 2.13 | 0.20 | 1.20 | 0.25 | Commercial |
| Slocum | 1.50 | 0.22 | 1.20 | 0.35 | Commercial |
| Seaglider | 2.00 | 0.30 | 1.00 | 0.25 | Commercial |
| SeaExplorer | 2.20 | 0.25 | 0.57 | 0.50 | Commercial |
| ANT Littoral | 1.83 | 0.32 | 1.10 | 1.00 | Commercial |
| OSUG | 1.12 | 0.11 | 0.82 | 0.20 | Open Source |
| USM | 1.30 | 0.17 | 1.00 | Unknown | Academic |
| ALBAC | 1.40 | 0.24 | 1.20 | 0.75 | Academic |
| STERNE | 4.50 | 0.60 | Unknown | 1.30 | Academic |
| ALEX | 1.00 | 0.085 | 0.82 | 0.30 | Academic |

Note. Data for Spray from Bluefin Robotics (2011), for Slocum from Teledyne Marine (n.d.), for Seaglider from Kongsberg Underwater Technology (2013), for SeaExplorer from Acsa Alcen (n.d.), for ANT Littoral from Exocetus Autonomous Systems (n.d.), for OSUG from Williams (n.d.), for USM from Underwater Glider Platform (n.d.), for ALBAC from Kawaguchi, Tomoda, Kobayashi, & Ura (1993), for STERNE from Graver (2005) and for ALEX from Arima, Ichihashi, & Miwa (2009).

### 1.3 Purpose of Thesis

It is possible to design an underwater glider with larger dimensions to accommodate more sensory equipment and more battery packs. On the other hand, we can also design a glider with minimal dimension to reduce drag. By reducing drag force, we can increase the range of the mission, reduce time taken for a specific mission, create enough energy budget for more sensors on board or increase sampling rate of the existing sensors. Correct design of an efficient underwater glider hull comes down to finding a good balance between a well-established internal space with enough volume and a low drag hull as well as the mission requirements. Moreover, dimensions and internal volume of gliders can also alter after the completed design of the glider by means of modular structure. Aim of this thesis is to find a relation between the volume of the water-tight body of an underwater glider and drag force acting on that body. By doing that we can have an understanding of what is gained or sacrificed by simply changing the diameter and the length of an underwater glider in terms of drag force. Such information would provide an easier and faster decision making in the preliminary design stages and would direct the designer to work on the right form or it could give us insight on new drag characteristics a glider after a module swap. To reach the results, two main sets of groups will be used; in the first one length of the glider will be kept constant and diameter will be changed, in the second one diameter of the glider will be kept constant and length of it will be changed. A constant cross section cylindrical center part with relatively short nose and back sections are commonly included in new hull designs (F. Myring, 1981). Therefore, both groups will be formed of torpedo shaped hulls. Torpedo shaped hull forms are very common in industry and academy and also they are easier to parameterize. Analyses will be run for three dimensional cases with different angle of attacks and OpenFOAM CFD package will be used for the analyses.

### 1.4 Literature Review

There have been several academic surveys for hydrodynamic analysis of an underwater gliders. Some of the research are experiment setups but majority of them use computational methods. Case setups and results of those research provide essential resource for constructing new cases.

Ichihashi, Ikebuchi, & Arima (2008), developed an underwater glider named ALEX to carry on towing tank experiments and CFD analysis. They performed model tests for velocities ranging from 0.5 to 0.8 m/s and attack angles ranging from -8 to 8 degrees in steps of two. For CFD studies they used RANS and continuity equations as governing equations, SIMPLEC scheme for pressure-velocity coupling and k-epsilon turbulence model. The mesh used for the study was an unstructured mesh with around 1 million cells for a 3D full body analysis. Ichihashi et al. (2008) reached similar results for Lift/Drag ratio from experiments and CFD analyses. This connects and compares a model experiment for gliders and CFD analysis it is an important criteria showing the health of computational methods. Later, Singh et al. (2017) reformed the CFD case to use ALEX glider as a validation point. They used SHIPFLOW 5.1.0 software to calculate RANS equations with a mesh 781914 of cells and used k-omega SST (Shear Stress Transport) turbulence model. Singh et al. (2017) stated that the work reached much closer value to the experiments done than the CFD results of Ichihashi et al. (2008) and related this result to the use of k–ω turbulence model rather than k- ε. The use of k-omega turbulence model improved CFD results in comparison to k-epsilon model. In 2015 Wang et al. (2015) conducted CFD analyses for a flying wing underwater glider. They acknowledged that the Reynolds number of the glider is in between the transition zone from laminar to turbulent, but as it is over limit of laminar boundary layer they made the assumption of fully turbulent flow and used k-ω SST turbulence model. This is an important assumption as Reynolds numbers for gliders in general fall into transition zone. Cao et al. (2015) conducted CFD tests for velocities 0.2 to 0.6 m/s and attack angles -14 to 14 degrees using FLUENT software with RANS, k-epsilon turbulence model. This study is also one of the studies that draws the line for range of velocities and attack angles. In a recent study, a glider with 2.35m length, 0.216m diameter has been designed and subjected to both model tests and CFD analyses by Liu et al. (2018). They used ANSYS FLUENT CFD software with RNG k-epsilon turbulence model and concluded that CFD result are in range of 2.5% error with experiments. Again showing level of error in making fully turbulent flow assumptions and using turbulence model accordingly.

# 2. APPLICATION OF COMPUTATIONAL FLUID DYNAMICS

## 2.1 Selection of Forms

To see the relationship between length, diameter, volume and drag force of a glider body, thirteen forms in two groups are prepared. These two groups are constant length with variable diameter and constant diameter with variable length. To create the dimensions for the CFD analysis, a base value for length and diameter parameters had to be chosen. By evaluating dimensions of commercial and academic gliders base values for watertight length and diameter are chosen as 1.50m and 0.20m respectively. Keeping these dimensions as basis, other forms are produced. One group of forms has a constant length of 1.50m with changing diameters and the other groups has a constant diameter of 0.20m with changing lengths. Because this study is interested in the relationship between internal volume of the glider and the drag force, watertight length of the body is taken as the main parameter rather than total vehicle length. Watertight length of a glider is the length of middle, parallel body section for a torpedo shaped glider. Nose and back sections are wet sections, they serve as a fairing rather than a container space so they are not included in the length parameter. Nose and back sections of the bodies are kept constant length and constant shape. Both nose and back forms are chosen to be Myring type. Myring type body consists of a middle cylindrical unit with a pair of nose and back units which are defined as a collection of semi-elliptic radius distributions (Hajivand, Mousavizadegan, Sadeghian, & Fadavi, 2016). The equation $r_1(x)$ for the nose (2.1) and $r_2(x)$ for the back (2.2) sections are as follows:

$$r_1(x) = \frac{1}{2}d\left[1 - \left(\frac{x-a}{a}\right)^2\right]^{\frac{1}{n}} \tag{2.1}$$

$$r_2(x) = \frac{1}{2}d - \left[\frac{3d}{2c^2} - \frac{\tan\theta}{c}\right](x-a-b)^2 + \left[\frac{d}{c^3} - \frac{\tan\theta}{c^2}\right](x-a-b)^3 \tag{2.2}$$

Where d is the diameter of center part, x is distance from the nose point to the back of the hull. The parameters a, b and c are length of the nose, center and back sections respectively. Variables $n$ and $\theta$ are geometric variables controlling fullness of the shapes. Larger the values of n and θ, the fatter the body becomes (Gao, Wang, Pang, & Cao, 2016). These parameters on the glider shape can be seen in the Figure 2.1. Effect of *n* and *θ* variables on the shape of the nose and back sections can be seen in the Figure 2.2 below.

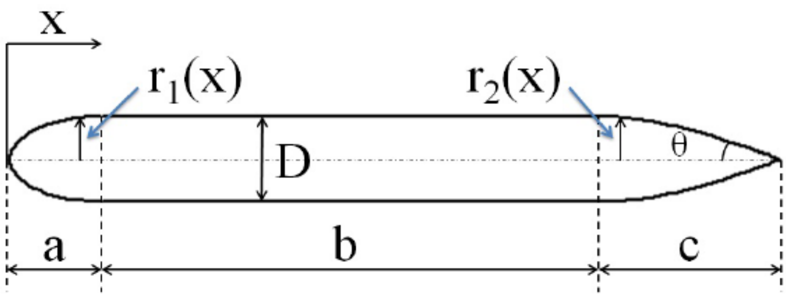


**Figure 2.1 :** Parameters of Myring Equation (Amorim Jr, 2014).

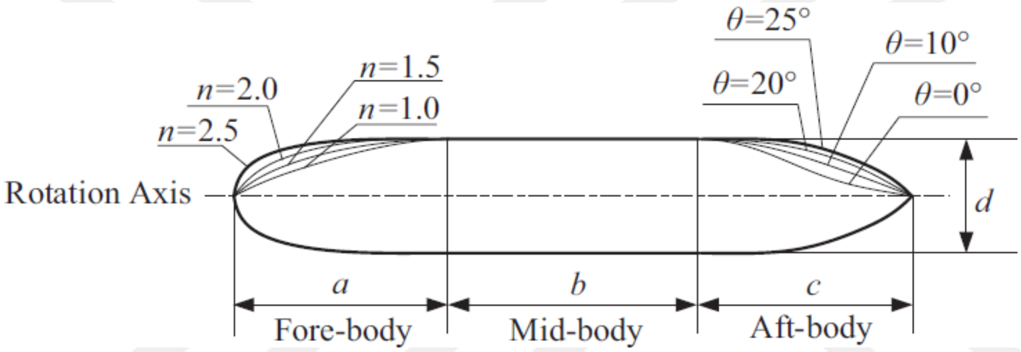


**Figure 2.2 :** Fore and aft body shapes depending on Myring equation, *n* and *θ* variables (hang Hou, Liang, & yang Mu, 2018).

For the purpose of this thesis, average nose and back shapes are constructed using *n* as 2 and *θ* as 20°. To keep the length of nose and back sections within range of the analyzed commercial and academic gliders, *a* and *c* parameters are chosen as 0.20 and 0.30 meters respectively. Two groups of selected forms can be seen in tables below. Table 2.1 shows forms with constant length and Table 2.2 show forms with constant diameter. Specifications for each form are given in the Table 2.3.

**Table 2.1 :** Forms of constant length.

| Length of Watertight Body (m) | Diameters of the body (m) |
|---|---|
| 1.50 | 0.12, 0.16, 0.20, 0.24, 0.28 |

**Table 2.2 :** Forms of constant diameter

| Diameter of the body (m) | Lengths of watertight body (m) |
|---|---|
| 0.20 | 0.50, 1.00, 1.50, 2.00, 2.50 |

**Table 2.3 :** Specifications of chosen forms.

| Form Number | Name of the Form | Diameter (m) | Watertight Length (m) | Total Length (m) | Watertight Volume ($m^3$) | Total Volume ($m^3$) | Wetted Area ($m^2$) |
|---|---|---|---|---|---|---|---|
| 1 | D0.20xL0.50 | 0.20 | 0.50 | 1.00 | 0.01571 | 0.02468 | 0.54824 |
| 2 | D0.20xL1.00 | 0.20 | 1.00 | 1.50 | 0.03142 | 0.04039 | 0.86240 |
| 3 | D0.20xL2.00 | 0.20 | 2.00 | 2.50 | 0.06283 | 0.07180 | 1.49072 |
| 4 | D0.20xL2.50 | 0.20 | 2.50 | 3.00 | 0.07854 | 0.08751 | 1.80488 |
| 5 | L1.5xD0.12 | 0.12 | 1.50 | 2.00 | 0.01696 | 0.02061 | 0.71201 |
| 6 | L1.5xD0.16 | 0.16 | 1.50 | 2.00 | 0.03016 | 0.03616 | 0.94311 |
| 7 | L1.5xD0.20 | 0.20 | 1.50 | 2.00 | 0.04712 | 0.05609 | 1.17656 |
| 8 | L1.5xD0.24 | 0.24 | 1.50 | 2.00 | 0.06786 | 0.08041 | 1.41278 |
| 9 | L1.5xD0.28 | 0.28 | 1.50 | 2.00 | 0.09236 | 0.10912 | 1.65211 |
| 10 | sL1.5xD0.12 | 0.12 | 1.50 | 1.80 | 0.01696 | 0.01890 | 0.64975 |
| 11 | sL1.5xD0.16 | 0.16 | 1.50 | 1.90 | 0.02867 | 0.03475 | 0.90379 |
| 12 | sL1.5xD0.24 | 0.24 | 1.50 | 2.10 | 0.06786 | 0.08336 | 1.46805 |
| 13 | sL1.5xD0.28 | 0.28 | 1.50 | 2.20 | 0.09236 | 0.11697 | 1.77827 |

Since the length of fore and aft sections are kept constant across all models, forms with larger diameter are expected to experience more flow separation at the back section. Therefore, to see how this can be corrected, four more forms are taken into consideration. This forms are created by scaling lengths of nose and back sections with respect to change in the diameter from the base diameter (for example, for a diameter of 0.24 m, nose and back sections are enlarged 20%). By doing that, total surface area of the model is expanded, but transition from parallel body to back section became more gradual. Form numbers 10 to 13 show specifications of these forms in the Table 2.3.

## 2.2 Preparation of Forms

Selected models are prepared using Rhinoceros 3D. Grasshopper plugin is used to procedurally generate all models without having to draw each one over. Figure 2.3, Figure 2.4 and Figure 2.5 show modelled forms with their respective form numbers. Dimensions of the forms with respect to each other are visualized in Figure 2.6.

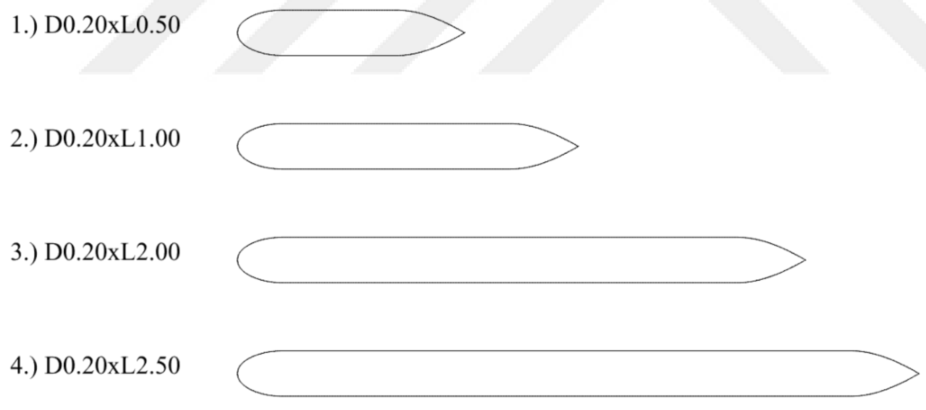


**Figure 2.3 :** Forms with constant diameter.

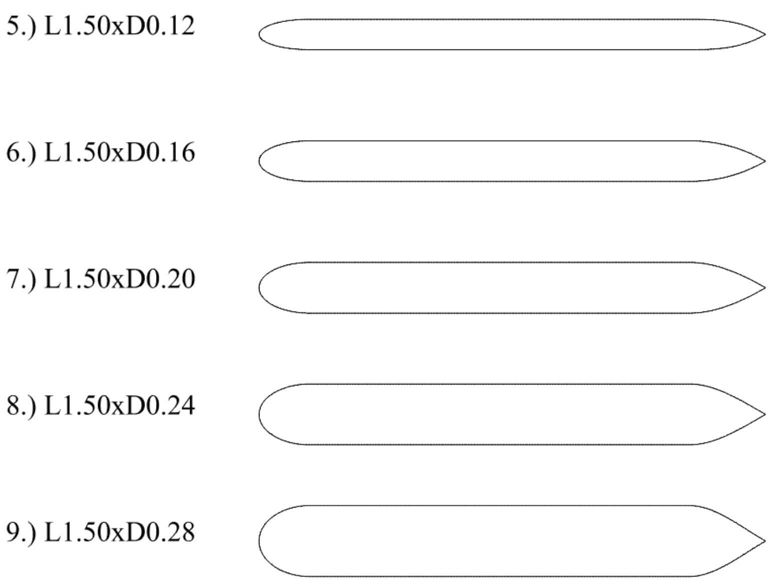


**Figure 2.4 :** Forms with constant length.

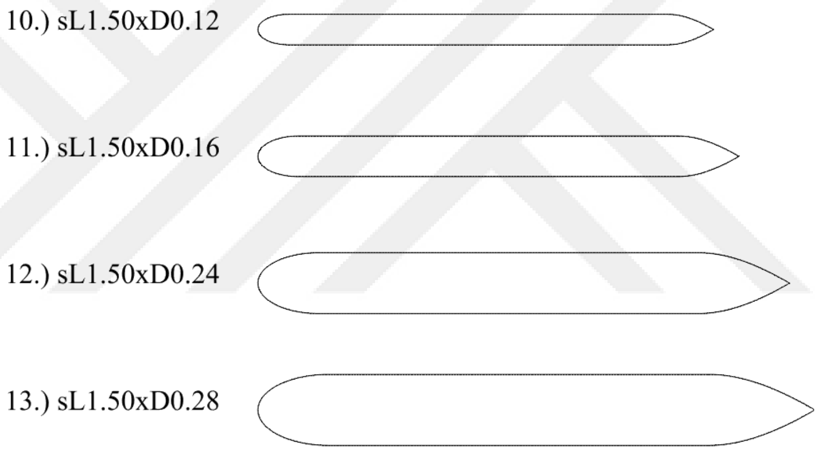


**Figure 2.5 :** Extra forms.

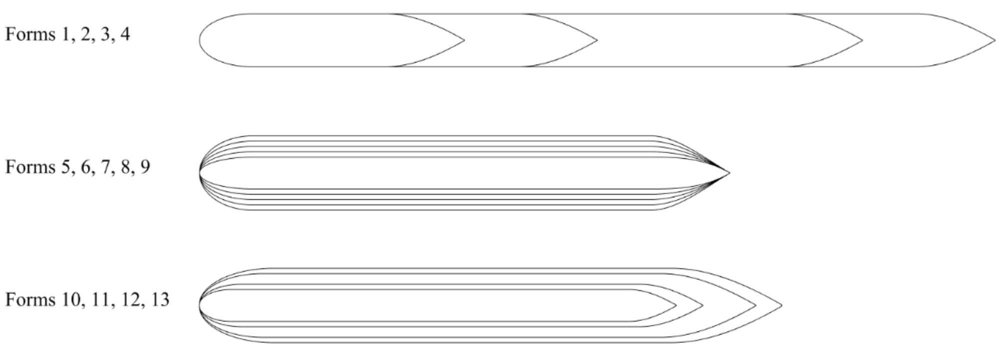


**Figure 2.6 :** Comparison of geometries.

Grasshopper plug in is used to draw the shapes and generate the information that is seen in the Table 2.3. Figure 2.7 below shows the established algorithm with the created body in the upper right corner. First creation of the algorithm takes some time but after that variables can be changed easily and different geometries can be visualized. All 78 geometries are created and evaluated this way (13 form in 6 different angles of attack).

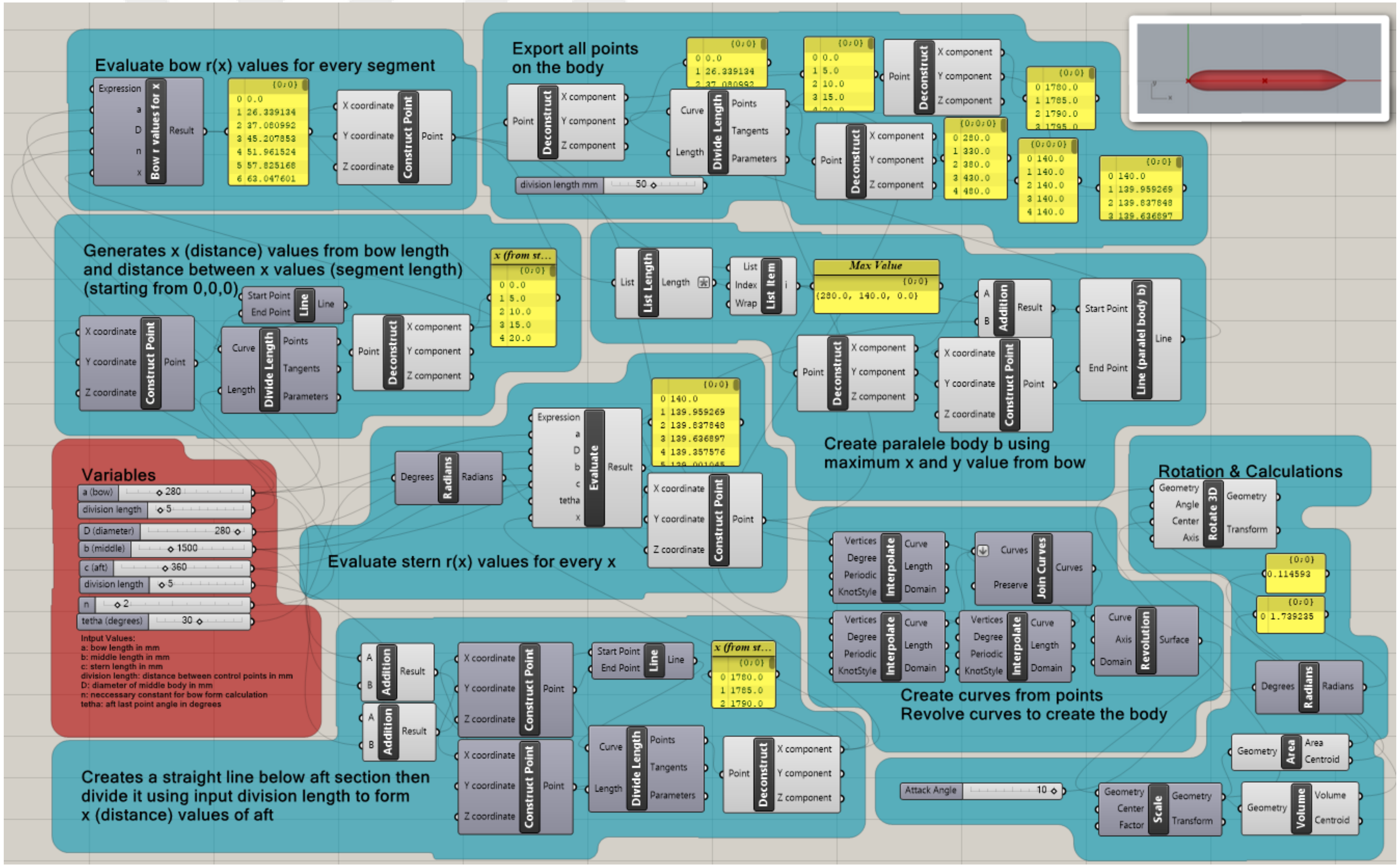


**Figure 2.7 :** Grasshopper algorithm for geometry preparation.

The OpenFOAM mesh utility *snappyHexMesh* requires either STL or OBJ format geometries. Therefore, geometries are exported in STL format. As quality of the output file effects mesh quality, a high quality mesh is generated using the export options. Maximum aspect ratio value is set to 1.00 and maximum distance of edge to surface parameter is set to 0.05 mm for the STL geometry.

### 2.3 CFD Parameters and Case Setup

In this study, 13 different asymmetric models are tested in 4 different velocities and 6 different angles of attack for a total of 312 different cases. Chosen velocities are 0.3, 0.6, 0.9 and 1.2 m/s, chosen attack angles are 0, 2, 4, 6, 8 and 10°. Velocities and attack angles are chosen in accordance with commercial and academic glider specifications. As gliders do not use a thruster, their velocities are generally in between 0.2 and 1 m/s. To resolve that range, velocities of 0.3, 0.6 and 0.9 m/s are chosen. 1.2 m/s is chosen to represent hybrid gliders with short term thruster use. Gliders can take advantage of attack angles ranging from -12 to 12° (for both ascent and descent) to make best use of their wings. However, -8 to 8° are more commonly used in the literature. Therefore, -10 to 10° range is chosen to represent attack angles. As the forms used in this study are axisymmetric hulls, only the positive region of attack angles are used. Analyses are done for every model in every velocity and attack angle totaling for 312 cases.

For the CFD analyses, OpenFOAM CFD software is chosen. OpenFOAM is an open source computational fluid dynamics software of the OpenFOAM Foundation and it was released by Mattijs Janssens, Chris Greenshields and Henry Weller in 2004 (OpenFOAM Foundation, n.d.). It supplies all the necessary tools for various kinds of CFD analyses and it is developed continuously with the modules created by developers and users. During the analysis of the cases in this thesis, incompressible flow assumption is made and the steady state solver (simpleFoam) of OpenFOAM is used. Steady state assumption is made to shorten and simplify the analyses. In the literature, many studies were carried out under the steady state assumption and they found accurate enough. Simulation type is chosen as RANS (Reynolds-Averaged-Navier-Stokes) and two-equation *k-ω SST* turbulence model is used. Minimum and maximum Reynolds numbers of the simulation cases can be seen from the Table 2.4. According to these Reynolds numbers, some of the cases fall into a region known as transition region between laminar and turbulent flows. Fully turbulent flow assumption for gliders is widely used in the literature and found appropriate in comparison to experiment results. Thus, in this study, a fully turbulent flow assumption is made for all cases and *k-ω SST* turbulence model is used rather than a transition turbulence model. Low Reynolds number approach is utilized for dimensionless wall distance value $y^+$ and it is kept between 0 and 1 in all cases.

**Table 2.4 :** Minimum and maximum Reynolds numbers.

| Form No | Name of the Form | Total Length (m) | Minimum Reynolds Number (0.3 m/s) | Maximum Reynolds Number (1.2 m/s) |
|---|---|---|---|---|
| 1 | D0.20xL0.50 | 1.00 | 2.99E+05 | 1.19E+06 |
| 2 | D0.20xL1.00 | 1.50 | 4.48E+05 | 1.79E+06 |
| 3 | D0.20xL2.00 | 2.50 | 7.46E+05 | 2.99E+06 |
| 4 | D0.20xL2.50 | 3.00 | 8.96E+05 | 3.58E+06 |
| 5 | L1.5xD0.12 | 2.00 | 5.97E+05 | 2.39E+06 |
| 6 | L1.5xD0.16 | 2.00 | 5.97E+05 | 2.39E+06 |
| 7 | L1.5xD0.20 | 2.00 | 5.97E+05 | 2.39E+06 |
| 8 | L1.5xD0.24 | 2.00 | 5.97E+05 | 2.39E+06 |
| 9 | L1.5xD0.28 | 2.00 | 5.97E+05 | 2.39E+06 |
| 10 | sL1.5xD0.12 | 1.80 | 5.37E+05 | 2.15E+06 |
| 11 | sL1.5xD0.16 | 1.90 | 5.67E+05 | 2.27E+06 |
| 12 | sL1.5xD0.24 | 2.10 | 6.27E+05 | 2.51E+06 |
| 13 | sL1.5xD0.28 | 2.20 | 6.57E+05 | 2.63E+06 |

Newtonian transport model with kinematic viscosity of 1.00481E-06 $m^2/s$ and density of 998.2 $kg/m^3$ are chosen as fluid properties. All cases were run for 1000 iterations. Before each run, *potentialFoam* utility of OpenFOAM is used to initialize the fields and utilize faster convergence. 20 non-orthogonal correctors for *potentialFoam* and 3 non-orthogonal correctors for *simpleFoam* are used to smooth mesh orthogonality related problems. In OpenFOAM, *nonOrthogonalCorrector* entry is used to fix orthogonality issues of mesh for given level. However, it increases calculation times of each time step considerably, thus it is a good idea to keep it to the minimum level necessary. Here, a lot of correctors (20) are specified for potential flow solver as it is very fast to solve. On the other hand, only 3 is assigned to the *simpleFoam* solver as the meshes used are not severely non-orthogonal. Forces, force coefficients, wall shear stress values, $y^+$ values and pressure coefficient values are recorded across all cases to be used in post-processing and to understand the health of the solutions.

Numerical schemes for terms are located in *fvSchemes* directory of OpenFOAM. When schemes are chosen, generally there is a tradeoff among stability, accuracy and required computational resource. In OpenFOAM, first order methods are bounded and stable but very diffusive, second order methods are accurate but might provide oscillatory results. All schemes used in this study are stable schemes with second order accurate results. A summary of used schemes for the analyses can be seen in the Table 2.5.

**Table 2.5 :** Summary of used discretization schemes.

| Names | Values | Notes |
|---|---|---|
| ddtSchemes | steadyState | Time discretization scheme for steady state condition. |
| gradSchemes | Gauss linear | Second order accurate scheme. |
| grad(U) | cellLimited Gauss linear | Velocity gradient computation to be used by div(phi,U). Used with a limiter for stability, less diffusive approach is taken by using cellLimited limiter. |
| divSchemes | default Gauss linear | Second order Gauss linear, the method is default for all unassigned terms. |
| div(phi, U) | bounded Gauss linearUpwind | Bounded second order scheme. |
| div(phi, k) | bounded Gauss linear | Second order accurate scheme. |
| div(phi, omega) | bounded Gauss linear | Second order accurate scheme. |
| laplacianSchemes | Gauss linear limited 0.33 | Second order scheme, usable with non-orthogonal correctors, when used with blending factor (0.33) gives higher accuracy sacrificing some stability. |
| interpolationSchemes | linear | Interpolation method of values from cell centers to face centers. |
| snGradSchemes | limited 0.33 | Same method and blending factor as laplacianSchemes. |

Linear solvers of variables are set from fvSolution directory. *GAMG* solver is used for pressure. For solving pressure equations in single phase cases, *GAMG* can be ideal solver ("Tips and tricks in OpenFOAM", n.d.). For other variables *smoothSolver* is selected. Results of *smoothSolver* is stable but slow. Since it is computationally less expensive to solve for *U, k* and *omega, smoothSolver* is found appropriate. Relaxation factor of 0.3 is used for pressure equations and 0.7 for *U, k* and *omega* equations.

Boundary and initial conditions are set under *U, p, k, omega* and *nut* directories inside *0* folder (meaning, time step 0). Boundary names for the domain are set as inlet, outlet, *ymin, ymax, zmin, zmax* and *glider*. Boundary conditions used in computations are listed in Table 2.6.

**Table 2.6 :** Boundary and internal field conditions for OpenFOAM.

| Boundary Name | Boundary Type | U | p | k | omega | nut |
|---|---|---|---|---|---|---|
| inlet | inlet | fixedValue *(internalField)* | zeroGradient $\nabla p=0$ | fixedValue *(internalField)* | fixedValue *(internalField)* | fixedValue uniform *(0)* |
| outlet | outlet | zeroGradient | fixedValue *(internalField)* $p=0$ | zeroGradient $\nabla k=0$ | zeroGradient $\nabla \omega=0$ | calculated |
| ymin | symmetry | symmetry | symmetry | symmetry | symmetry | symmetry |
| ymax | symmetry | symmetry | symmetry | symmetry | symmetry | symmetry |
| zmin | symmetry | symmetry | symmetry | symmetry | symmetry | symmetry |
| zmax | symmetry | symmetry | symmetry | symmetry | symmetry | symmetry |
| glider | wall | fixedValue uniform *(0 0 0)* | zeroGradient $\nabla p=0$ | fixedValue uniform *(very small number)* | omegaWallFunction *(internalField value)* | fixedValue *uniform* *(very small number)* |
| internalField | internalField | uniform *(velocity value)* | uniform *(0)* | uniform *(turbulentKE)* | uniform *(turbulentOmega)* | uniform *(0)* |

## 2.4 Mesh Creation

Meshes for models are created using OpenFOAM utilities *blockMesh* and *snappyHexMesh*. For creating computational domain and naming boundaries, *blockMesh* utility is used. After that, models are meshed using *snappyHexMesh* utility. Finally, before analyses, quality of the meshes are checked for possible problems. As analyses forms are axisymmetric, symmetric domains and bodies are used to save computational time. Therefore, all analyses were done using half body symmetry.

Computational domain is prepared in Rhinoceros 3D using Grasshopper plugin. Domain coordinates are exported and used in *blockMeshDict*. Figure 2.8 shows the Grasshopper algorithm used for domain and refinement zone visualization. Foremost point (tip of the head) of the model is placed onto origin with vehicle length lying towards positive x-direction. A computational domain is created large enough so that it can be used for every model. Boundaries of domain lie 5 meters towards negative x-direction, 20 meters toward positive x-direction and 5 meters in every other direction. Visualization of domain can be seen in the Figure 2.9.

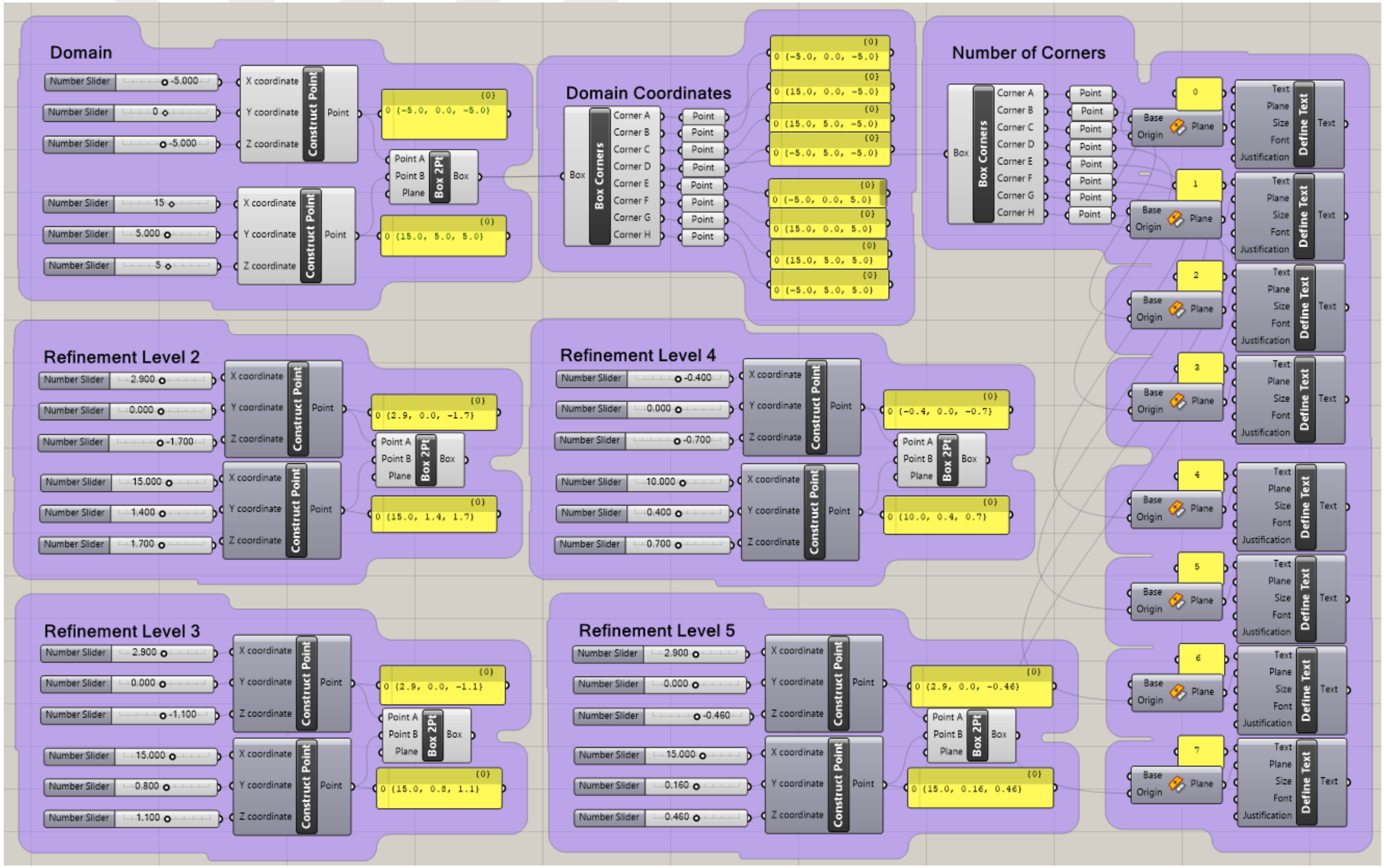


**Figure 2.8 :** An example of Grasshopper algorithm for domain and refinement zone visualization.

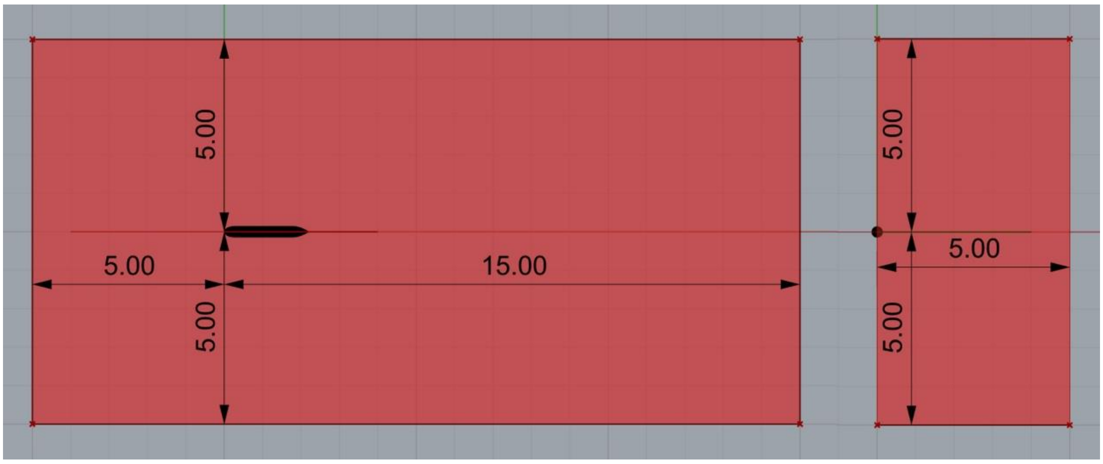


**Figure 2.9 :** Dimensions of domain.

The initial decomposition of the domain for *x*, *y* and *z* axis is done in the *blockMeshDict*. This mesh creates the level 0 base mesh for the refinements to build upon. Increasing the division numbers in the *blockMeshDict* results in a finer base mesh and also results in a finer mesh in the refinement regions without changing their levels. The final mesh is constructed with 5 refinement levels in domain and a boundary layer refined enough for $y^+$ values of around 1. In the Figure 2.10, Figure 2.11 and Figure 2.12 below, details of the final mesh generated for the half body setup is given. The meshing parameters set from *snappyHexMeshDict* are either same or quite similar for every geometry so, mesh generation work is largely automatized for all 78 meshes (13 models in 6 different angles).

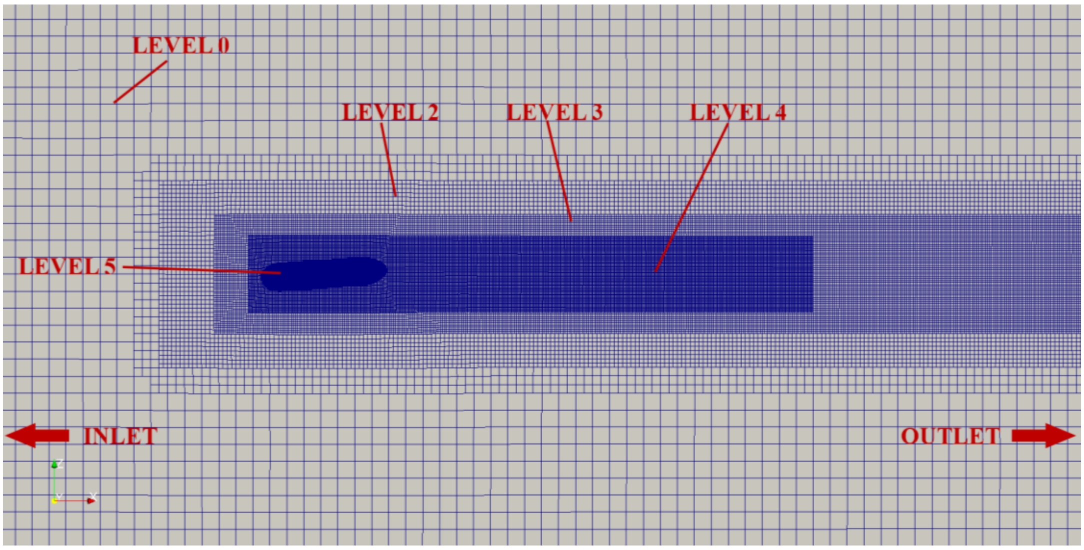


**Figure 2.10 :** Mesh topology of the domain.

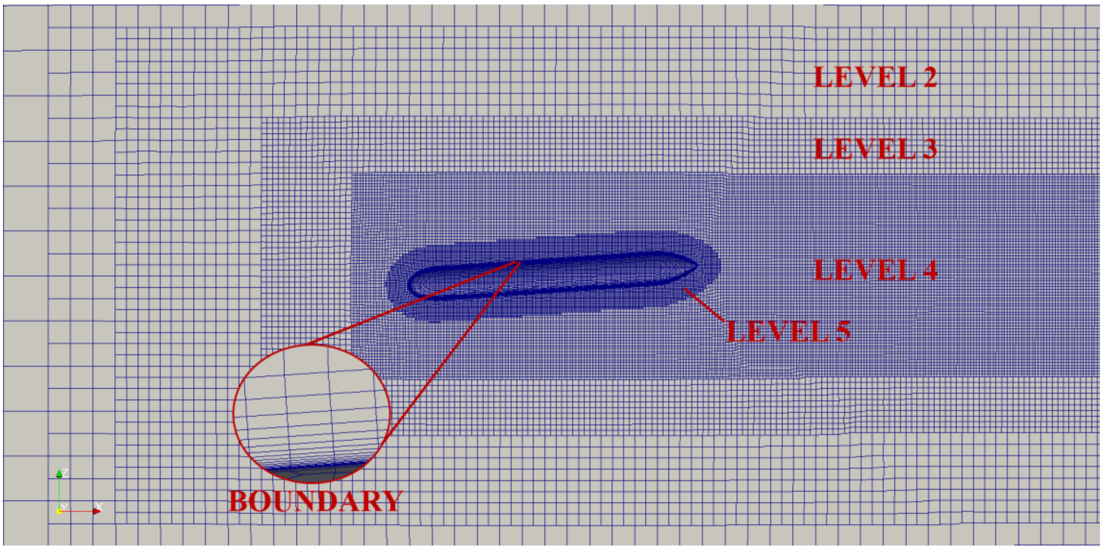


**Figure 2.11 :** Mesh topology around the body.

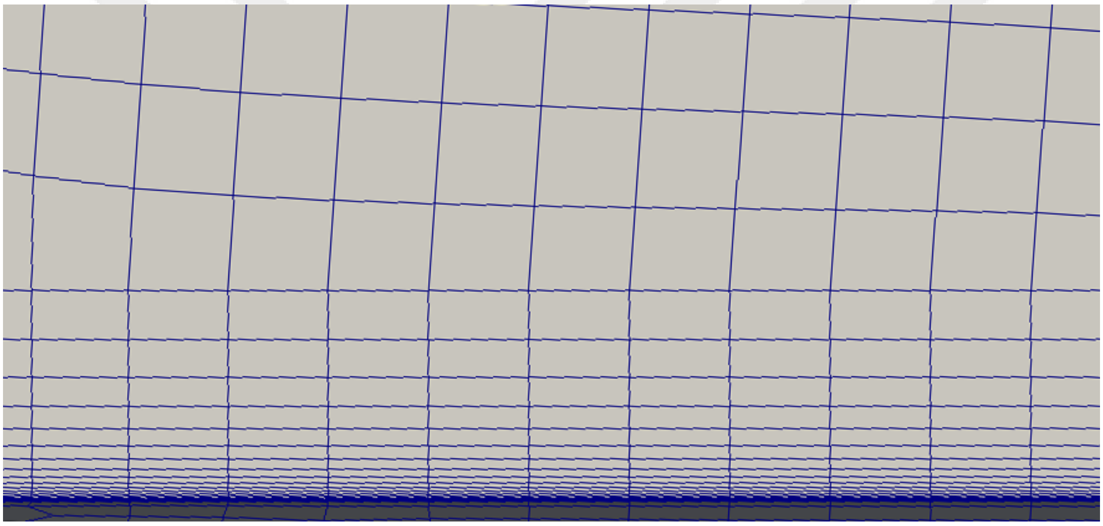

**Figure 2.12 :** Boundary Layer.

To understand the relation of the solutions with fineness of the mesh, a mesh independence test is conducted. Therefore, first, a mesh outline with the levels and parameters explained above is created to set a suitable relation between sub-refinement zones. Then, decomposition numbers for the base mesh are set inside the *blockMeshDict*. Using this setup, fineness of the final mesh can be controlled by changing the initial decomposition numbers of base mesh without disturbing relations between sub refinement zones. Initially, a very coarse mesh is created, then finer meshes are created with the settings that produce around 2 times the number of cells of the previous fineness. The reference model (0.2m diameter, 1.5m watertight length) in 0° attack angle is used for the test. Tests are run for 0.6 m/s velocity. A total of 5 meshes are used in the mesh independence test with the labels very coarse, coarse, medium, fine and very fine. Drag force results are collected to make the comparison between meshes. Table 2.7 includes particulars of the results as a summery and Figure 2.13 represents change in drag force with number of cells. Drag forces are nondimensionalized using density, velocity and surface area of the glider to find the drag coefficients.

**Table 2.7 :** Values of mesh independence study.

| Fineness | Number of Cells | Pressure Drag (N) | Viscous Drag (N) | Total Drag (N) | $C_D$ |
|---|---|---|---|---|---|
| Very Coarse | 301892 | 0.528 | 0.832 | 1.360 | 6.435E-03 |
| Coarse | 546316 | 0.212 | 0.860 | 1.071 | 5.068E-03 |
| Medium | 1165404 | 0.159 | 0.858 | 1.017 | 4.809E-03 |
| Fine | 2423892 | 0.135 | 0.860 | 0.995 | 4.708E-03 |
| Very Fine | 4933008 | 0.120 | 0.860 | 0.980 | 4.638E-03 |

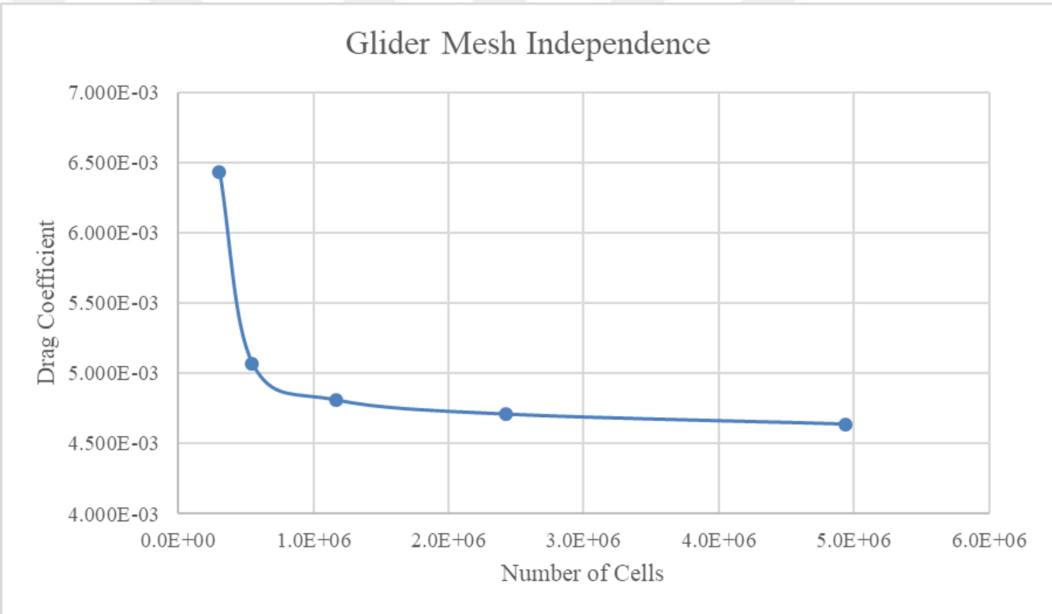


**Figure 2.13 :** $C_D$ values with respect to number of cells.

When change in the force and computational expensiveness of the cases are compared “fine” level mesh is taken as the appropriate reference. All the meshes are formed in the formation of “fine” level mesh with minor adjustments.

After the meshing stage, the meshes are checked for problems using OpenFOAM utility *checkMesh* and *meshQualityDict.* All meshes used in the analyses passed the quality checks. Major mesh quality check parameters are orthogonality, skewness, aspect ratio and face orientation. For all cases, maximum non-orthogonality parameter was around 55 (acceptable limit for *checkMesh* utility is below 65), maximum skewness parameter was around 1 (acceptable limit for *checkMesh* utility is below 4), maximum aspect ratio was around 200 and found appropriate. Lastly, number of incorrectly oriented faces which may create problems in flow were below 10.

### 2.5 Verification of CFD Parameters

To verify the capability and suitability of the chosen CFD setting, a well-known case which could allow us to make sure of the results is required to be chosen. For this reasons, DARPA Suboff bare hull model and cases are selected to be verified. Main dimensions of the bare hull version of the DARPA Suboff geometry are given in the Table 2.8 and in the Figure 2.14 Suboff geometry can be seen. Analyses are conducted for 7 different velocities. Velocity of 3.046, 5.144, 6.091, 7.161, 8.231, 9.255 m/s are chosen to compare drag force acting on the body and 3.34 m/s is used to compare $C_P$ graphs. All CFD parameters are kept the same as the ones determined for the glider. Mesh topology and fineness are also the same as glider cases. The results are compared to experimental study results of Liu & T. Huang (1998).

**Table 2.8 :** Dimensions of DARPA Suboff (C. Groves, T. Huang, & S. Chang, 1989).

| Paramater | Value |
|---|---|
| L (m) | 4.356 |
| $D_{max}$ (m) | 0.508 |
| S ($m^2$) | 5.988 |

**Figure 2.14 :** DARPA Suboff geometry without appendages.

For the velocity of 5.144 m/s, drag force results are listed in the Table 2.9. In the Figure 2.15 $C_P$ curves for the velocity of 3.34 m/s are given with respect to experiment result taken from the work of Sezen, Dogrul, Delen and Bal (2018).

**Table 2.9 :** CFD result for velocity of 5.144 with respect to experiment for DARPA Suboff.

| Velocity | Number of Cells | Total Drag (CFD) | Total Drag (Experiment) | Error |
|---|---|---|---|---|
| 3.046 | 1.2 M | 85.4 | 87.4 | 2.29% |
| 5.144 | 1.2 M | 232.2 | 242.2 | 4.13% |
| 6.091 | 1.2 M | 316.6 | 332.9 | 4.90% |
| 7.161 | 1.2 M | 427.9 | 451.5 | 5.23% |
| 8.231 | 1.2 M | 556.3 | 576.9 | 3.57% |
| 9.255 | 1.2 M | 713.7 | 697 | 2.40% |

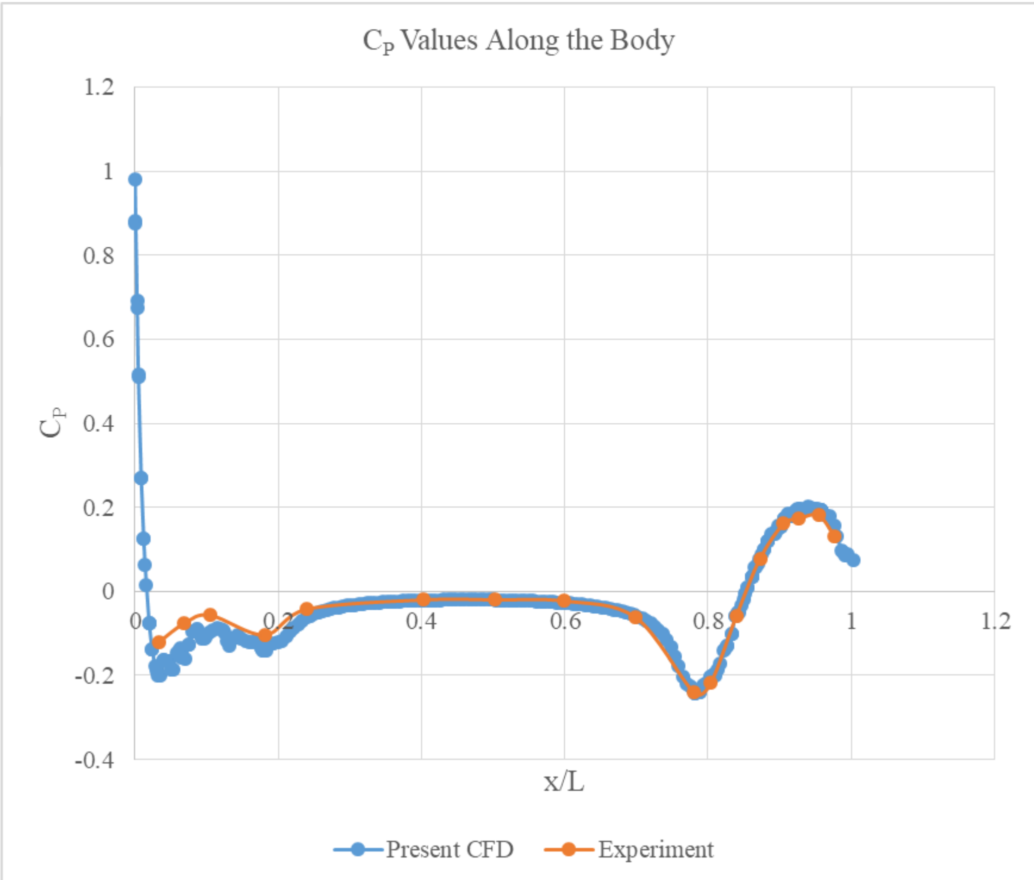


**Figure 2.15 :** Comparison of $C_P$ values for CFD and experiment for DARPA Suboff.

# 3. RESULTS AND DISCUSSION

Results of the study were analyzed in Paraview software. First, dimensionless wall distance parameter $y^+$ values are checked to see if preliminary assumptions on boundary layer are correct. In all cases, $y^+$ values smaller than 1 were achieved. Figure 3.1 shows an example distribution of $y^+$ over the hull of Form 13 for 0.6 m/s velocity. Wake lines for models are captured in full length of domain (Figure 3.2)

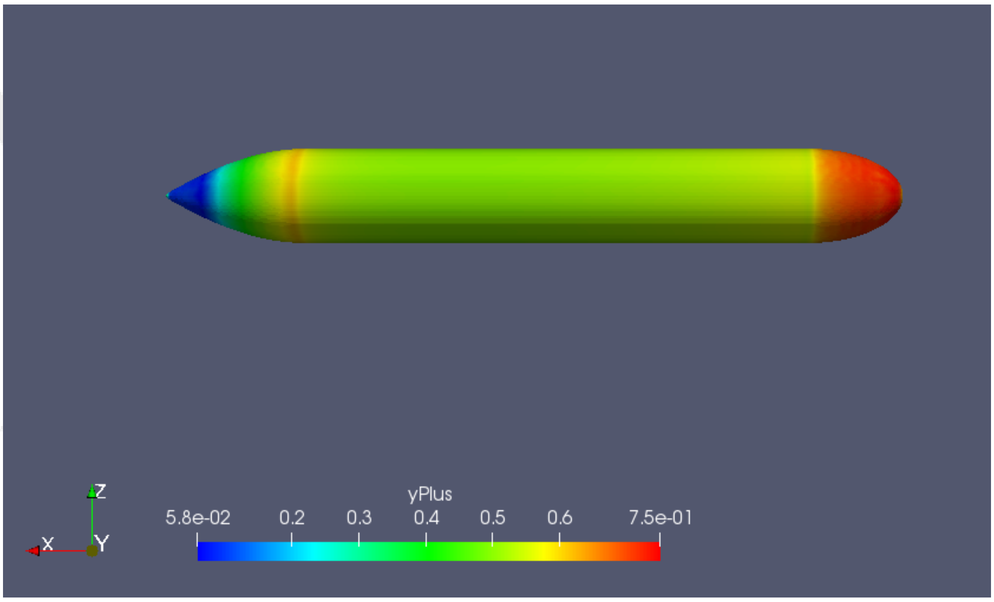


**Figure 3.1 :** $y^+$ value distribution over Form 13.

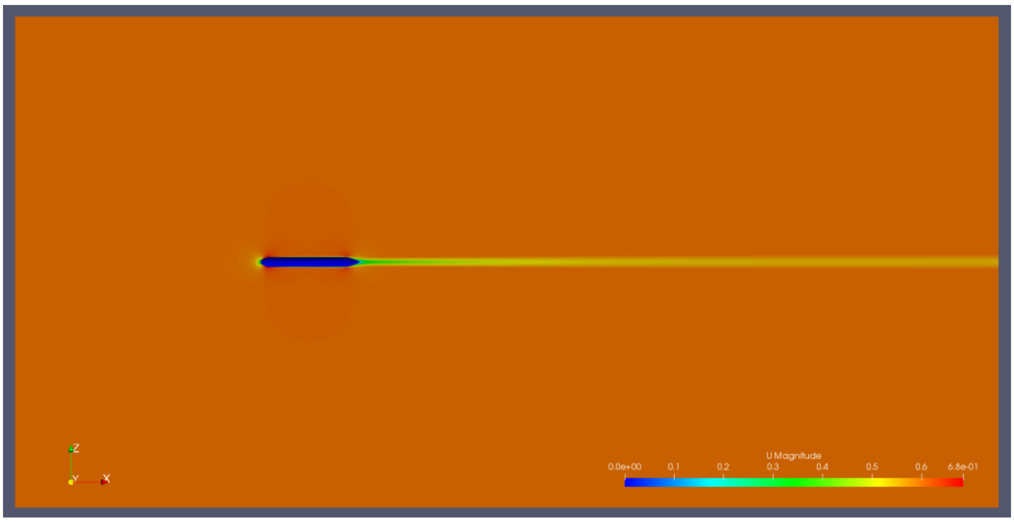

**Figure 3.2 :** Wake line through domain.

Other result regarding attack angle, velocity, volume and drag are summarized below using attack angles 0, 6, 10° and velocities 0.3, 1.2 m/s. Results are grouped using the initial groups of constant diameter and constant length. For graphs a fitting trend line is used to help interpret the data points better. Figure 3.3 shows velocity profile of Form 1 in different attack angles and velocities. Same velocities share the same scale throughout all figures of velocity and pressure profiles.

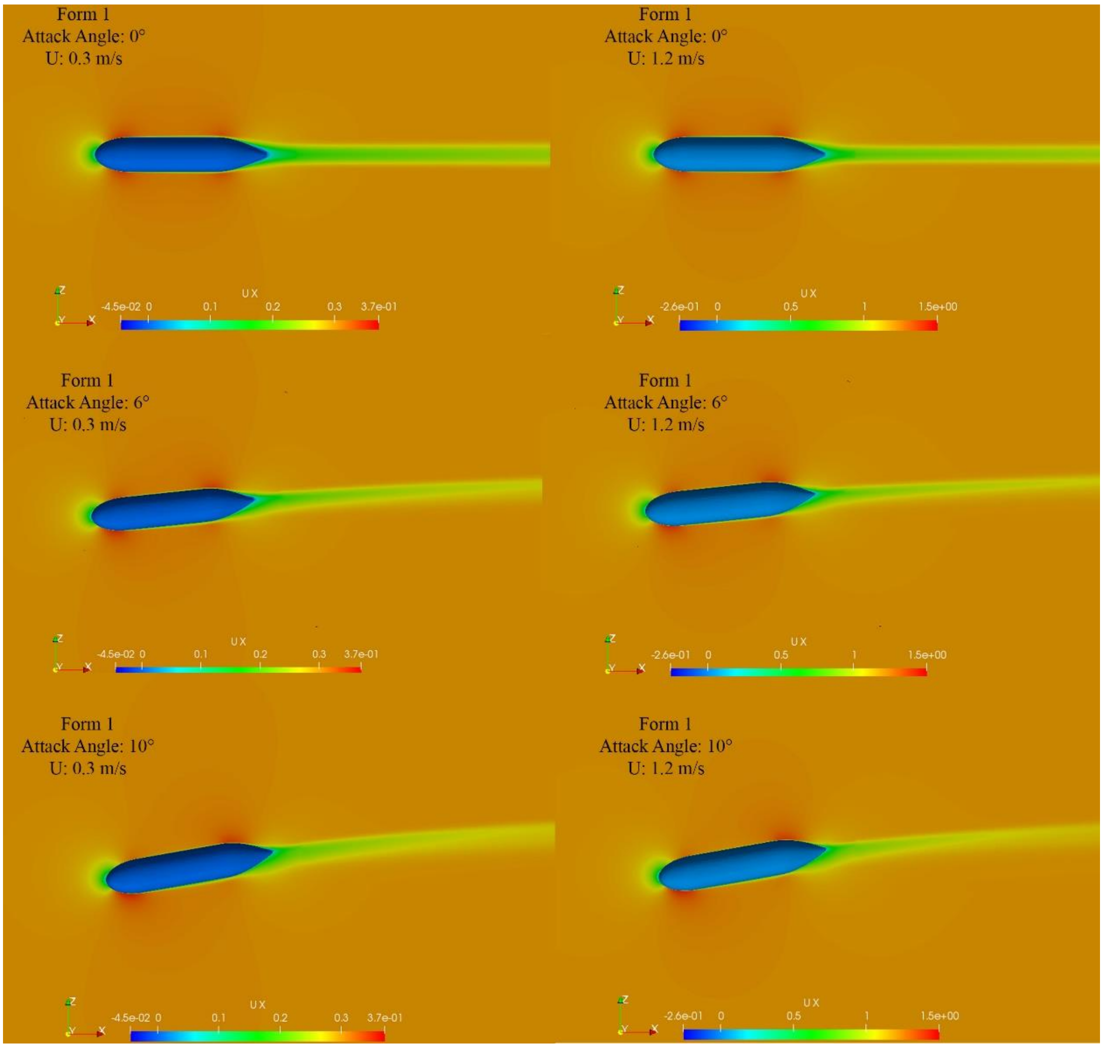


**Figure 3.3 :** Velocity profiles for Form 1.

Change in drag coefficient with respect to L/D ratio for two groups are given in the Figure 3.4 below. Forms with constant diameter of 0.20m is on the left side and forms with constant length of 1.50m are on the right side of the figure. It can be seen that as the slenderness (L/D) increases drag coefficient decreases for all geometries. For the constant length cases it can be said that L/D ratio of more than 8 has little impact on drag characteristic of the vehicle. Therefore it would not be useful to design very slender vehicles in that range. In the third group of forms (Forms 10, 11, 12, 13), lengths of nose and back sections are scaled according to diameter change from the base form (L1.50xD0.20m, Form 7). This created a more stable $C_D$ profile change with increasing slenderness (Figure 3.5) even though these forms create more drag force through having longer $L_{OA}$.

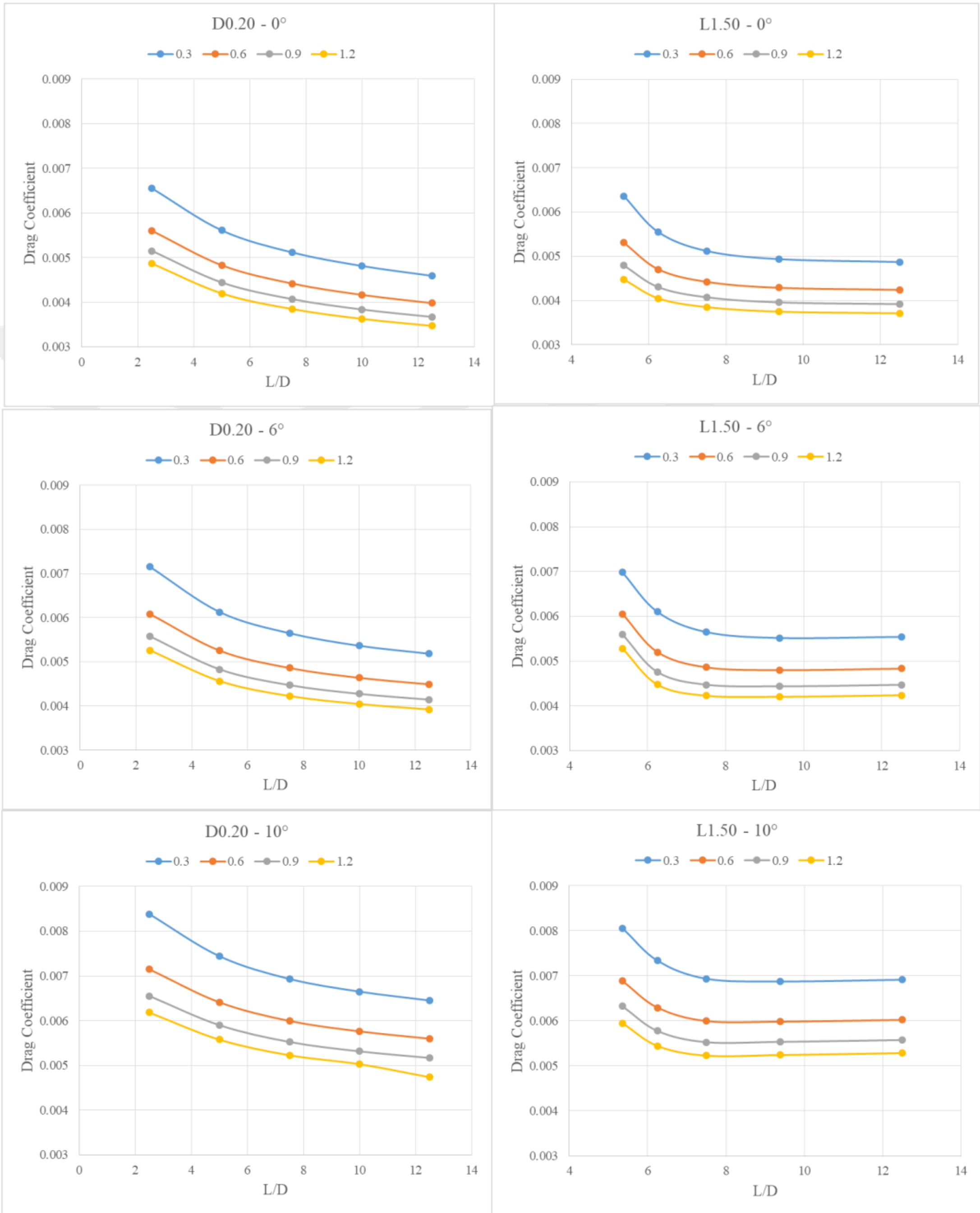


**Figure 3.4 :** $C_D$ with respect to L/D for Forms 1-10.

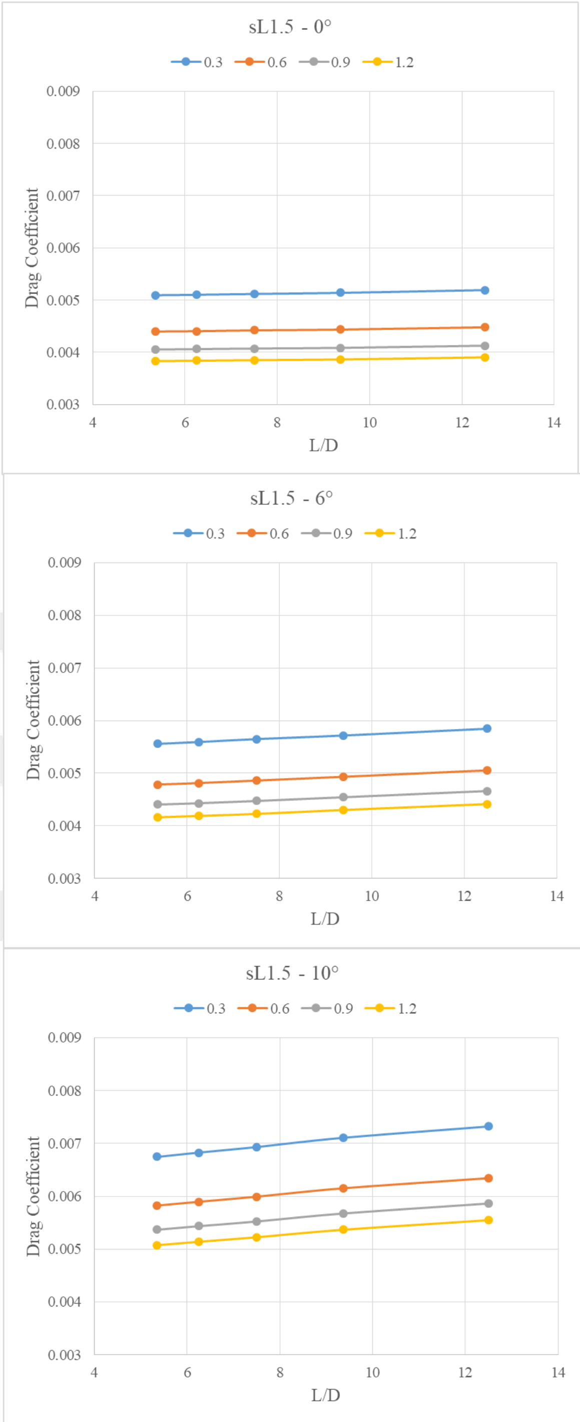


**Figure 3.5 :** $C_D$ with respect to L/D for Forms 10-13.

Value of drag force (N) with respect to watertight volume ($m^3$) are given in the Figure 3.6 for Forms 1-4 and in Figure 3.7 for Forms 5-13. It is clear that increasing volume affects drag force worse in higher velocities by far. Till the vehicle passes 0.6 m/s, volume change does not contribute much to drag increase. When the information from these figure are combined with the information from Figure 3.8, a comment on the a effect of diameter of the hull to the drag force created as a result of separation can be made. Figures 3.8 shows viscous drag – pressure drag ratio with respect to change in the slenderness of the hull.

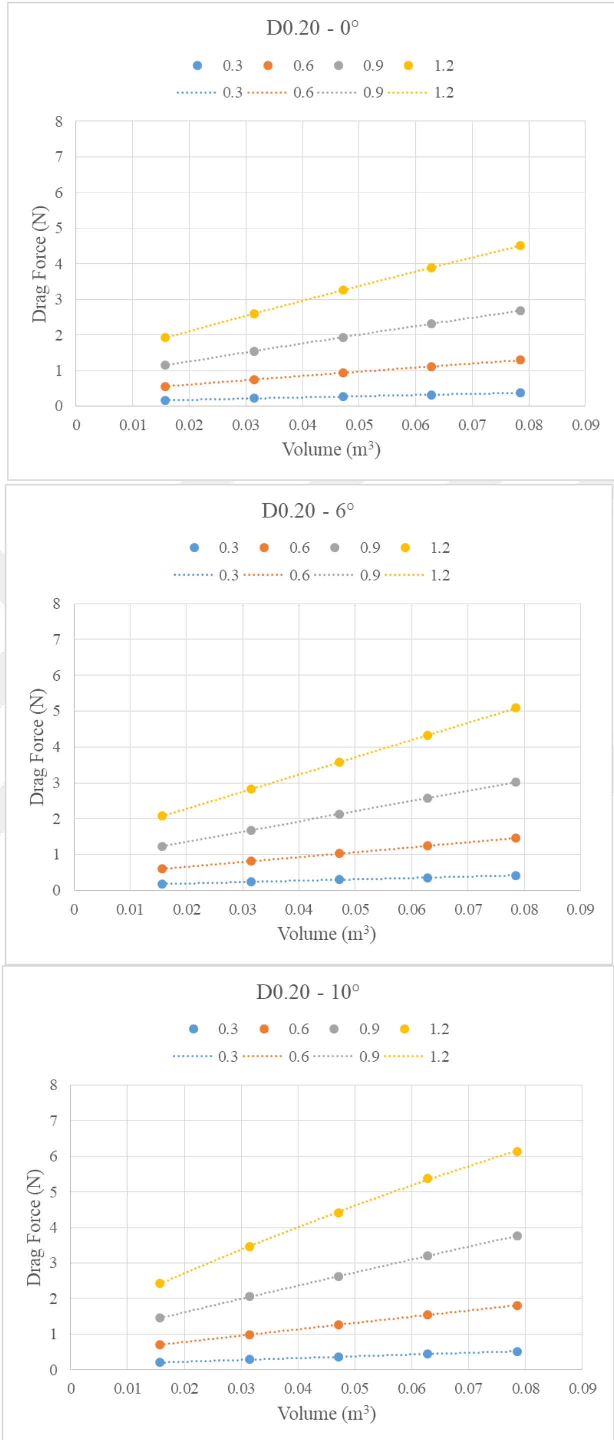


**Figure 3.6 :** Drag force with respect to volume of watertight body for Forms 1-4.

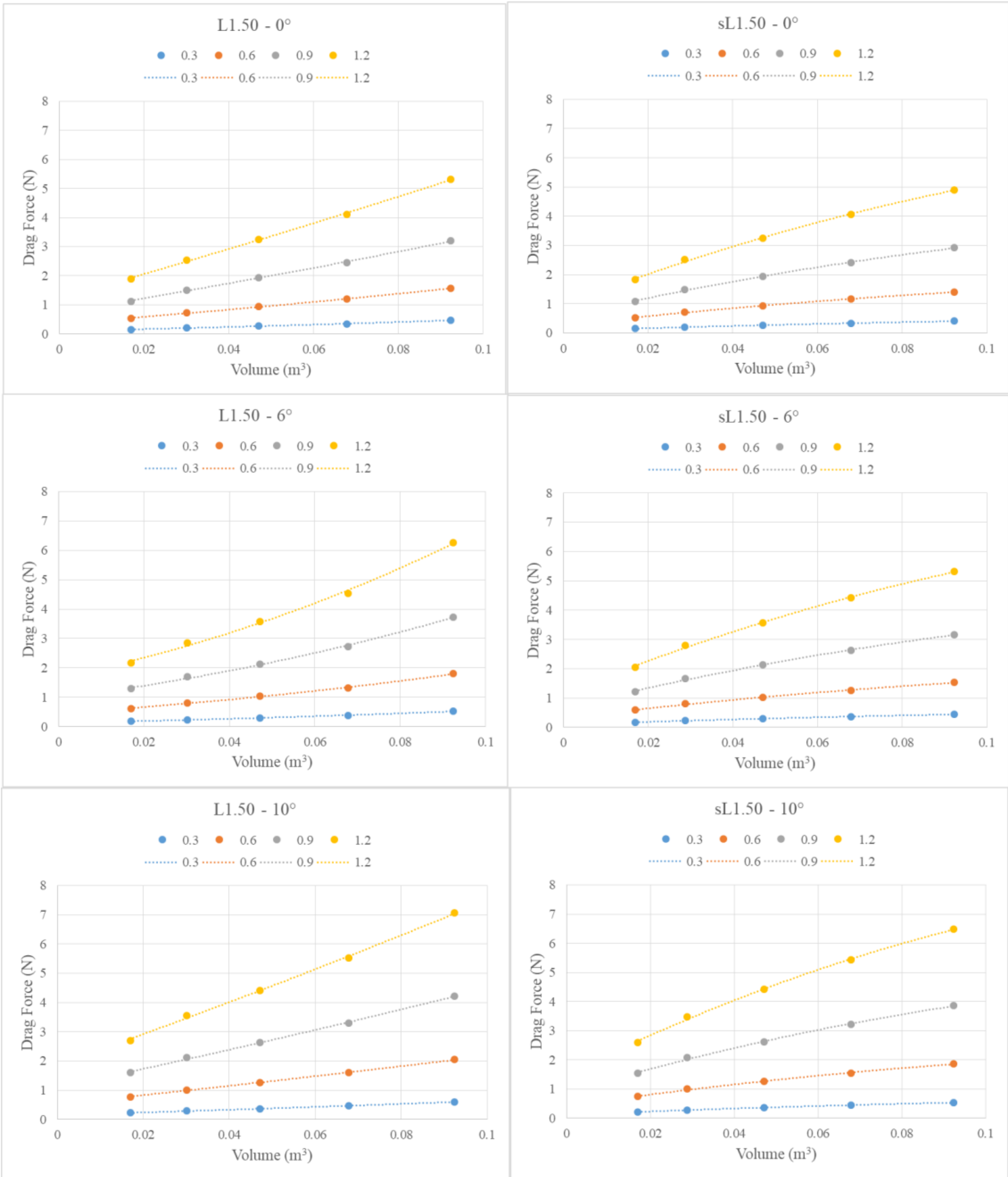


**Figure 3.7 :** Drag force with respect to volume of watertight body for Forms 5-13.

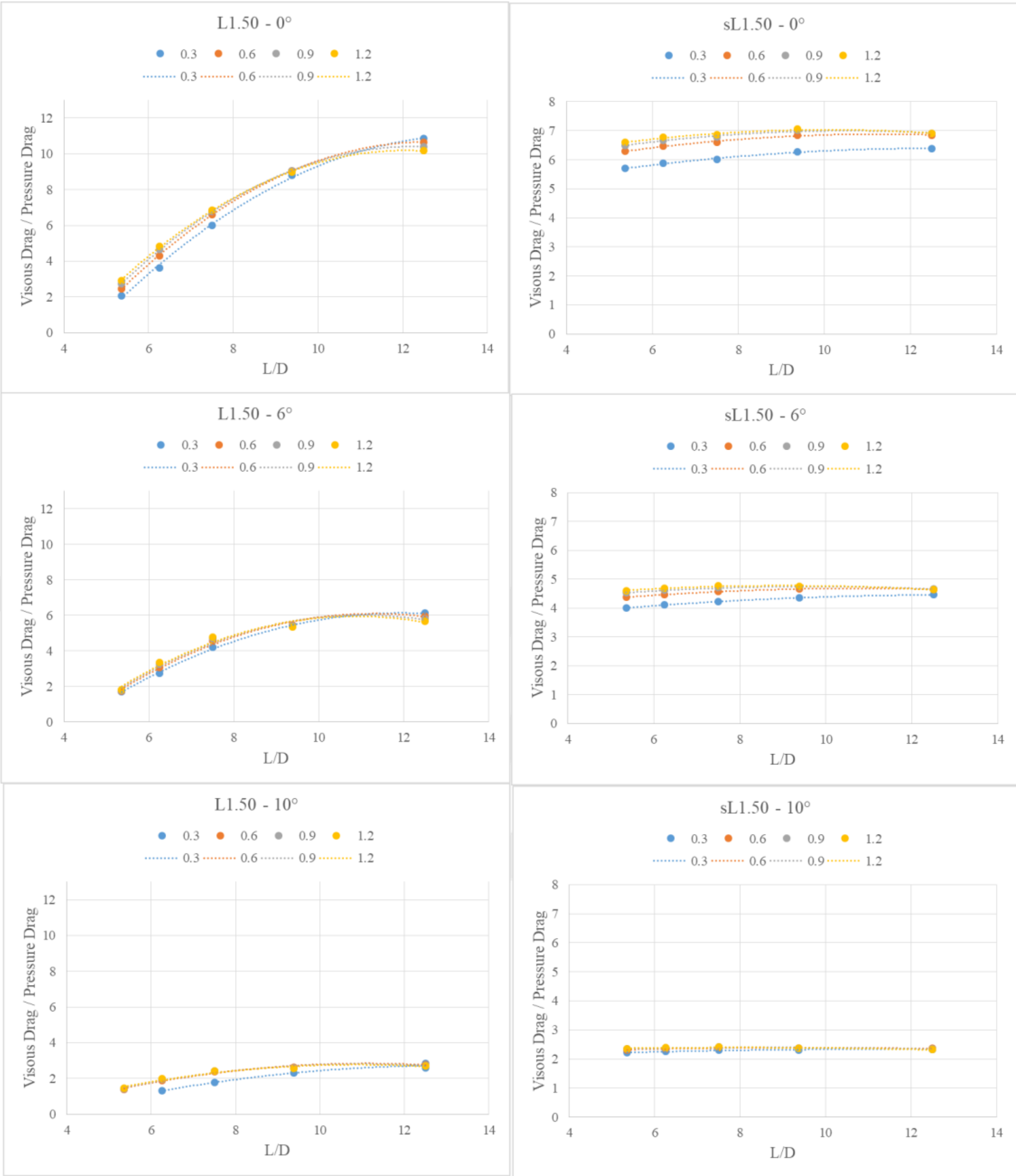


**Figure 3.8 :** Viscous drag to pressure drag ratio with respect to L/D.

As it can be seen from Figure 3.8, L/D ratio does not change the ratio between drag components much for "sL1.50" cases (Forms 10 through 13). "sL1.50" forms are longer than "L1.50" forms therefore viscous drag component is larger. However, the change in L/D ratio does not account for a big change in pressure drag as the hull forms is getting smaller smoothly in "sL1.50" forms. Whereas change of the form for "L1.50" geometries are more sudden and cause higher pressure drag for lower L/D ratios even in the smaller angle of attack range. As the attack angle gets bigger, nose and back forms gets a little less important as pressure drag is already high from the attack angle related separation. When this figure is compared to Figure 3.7, the victory of smoother form over the drag force can be seen more clearly. In Figure 3.7, for all cases of "sL1.50" forms the total drag force is smaller than the "L1.50" forms except 0.3 m/s velocity for all attack angles. Furthermore, this advantage further increases with higher velocities and attack angles.

## 4. CONCLUSION

Underwater gliders are unmanned underwater vehicles that can move underwater by changing their buoyancy and center of gravity. They do not utilize a propulsion system to maneuver, thus they are extremely energy efficient. Depending on its mission, an underwater glider can actively work underwater around 6 to 12 months. This endurance makes them ideal for gathering data over long periods and great distances. To further increase mission capabilities, range or speed of an underwater glider, it is important to design a low drag hull form. A low drag hull form can be designed by keeping dimensions of the hull as small as possible. However, internal space of a glider is an important limiting factor in determining hull dimensions. Volume of the battery inside the glider hull directly effects its endurance and range. Therefore a good balance must be ensured between hull drag and internal volume of a glider.

In this study, it is aimed to find the relationship between displacement volume of an underwater glider and the respective drag force acting on it. This relationship can be integrated into design stage to determine the optimal form faster. Moreover, for modular gliders, this information can provide an insight on the respective change of drag of the vehicle after a module change.

To satisfy this purpose 13 hull forms with torpedo body are created according to dimensions of commercial and academic gliders. Forms are grouped under constant diameter or constant length parameters to factor in separate effects of length and diameter on drag force. CFD analyses were done using OpenFOAM CFD software. Steady state approach and k-omega SST turbulence model were chosen as the CFD parameters. Half body symmetry was used in all analyses to lower computational time. For a better low Reynolds number approach, $y^+$ values for analyses were kept lower than one. To verify the mesh topology and fineness, a mesh independence test was performed. To verify CFD methods and solver parameters used in the OpenFOAM, analyses on DARPA Suboff bare hull form were conducted using the verified mesh topology. These test verified and finalized the mesh and CFD parameters.

Analyses on 13 hull forms were executed for velocities ranging from 0.3 to 1.2 m/s and for attack angles ranging from 0 to 10°. A total of 312 analyses were done and the results are given comparing drag force, drag coefficient, volume and length-diameter ratio in relationship with each other.

Analyses results show that volume change contributes to drag force greatly for higher velocities and for higher attack angles. For velocities in the range of 0.3 to 0.6 m/s a vehicle with a bigger volume does not cause a severe increase in drag force. Therefore, It can be said that gliders without a propeller to be used in a hybrid case may not get hurt as much from a bigger hull and may be much more useful in a modular design scenario.

Overall, it is a good idea to keep length and diameter down to reduce the viscous and pressure drag forces. However for bigger diameters that reduce the L/D ratio greatly, it could be a good idea to consider reforming front and back fairings to reduce separation, even if it means making a longer vehicle overall. Therefore there are no other limits present experimenting with a more gradually changing nose and back sections could provide lower overall drag force, especially for gliders that utilize a bigger attack angle.

It is generally an acceptable strategy to increase slenderness of the vehicle while increasing the total volume. However, the results show that after L/D ratios of 10-12 the effect diminishes. High L/D ratios create higher footprint areas which is not desirable for glider carried on a ship (since it would make packing of a fleet of gliders together on board of a ship harder). Hence it can be useful to keep L/D ratios around or below 10.

In this study, drag force on the bare hull of a glider is inspected, but there are several appendages on a glider that may create considerable drag such as sensory packages, wings and antennas. Therefore, a similar study for scenarios of complete underwater gliders can be experimented.

Drag force is one parameter affecting the efficiency of a glider. Chen et al. (2014) states that underwater glider performance cannot be assessed only by the drag force, but energy consumption is one of the crucial elements as well. Parameters such as battery pack size, efficiency of internal engines, diving depth and density of the water affect efficiency and mission performance of a glider. A study that factors in one or more of those parameter could give a more realistic view on glider design. Such a study would contain a lot of assumptions and may not be practical, but in the long term it could create an important piece of information that can be used for a more complete understanding and better design of small autonomous underwater vehicles.

## REFERENCES

**Acsa Alcen.** (n.d.). Seaexplorer. [PDF file]. Retrieved from http://auvac.org/uploads/platform_pdf/ACSA_SeaExplorer_Datasheet.pdf

**Amorim Jr, W.** (2014). Numerical Analysis of Turbulent Fluid Flow and Drag Coefficient for Optimizing the AUV Hull Design. *Open Journal of Fluid Dynamics, 4, 263–277.*

**Arima, M., Ichihashi, N., & Miwa, Y.** (2009). *Modelling and motion simulation of an underwater glider with independently controllable main wings.* In *OCEANS '09 IEEE Bremen: Balancing Technology with Future Needs. https://doi.org/10.1109/OCEANSE.2009.5278267*

**Bluefin Robotics.** (2011). Bluefin spray glider. [PDF file]. Retrieved from http://auvac.org/uploads/platform_pdf/Bluefin-Spray-Glider-Product-Sheet.pdf

**C. Groves, N., T. Huang, T., & S. Chang, M.** (1989). Geometric Characteristics of DARPA (Defense Advanced Research Projects Agency) SUBOFF Models (DTRC Model Numbers 5470 and 5471), 82.

**Cao, J., Cao, J., Yao, B., & Lian, L.** (2015). Three dimensional model, hydrodynamics analysis and motion simulation of an underwater glider. *OCEANS 2015 - Genova*. https://doi.org/10.1109/OCEANS-Genova.2015.7271365

**Chen, Y. J., Chen, H. X., & Ma, Z.** (2015). Hydrodynamic analyses of typical underwater gliders. Journal of Hydrodynamics, 27(4), 556-561.

**Davis, R., Eriksen, C., & Jones, C.** (2002). Autonomous buoyancy-driven underwater gliders. *Applications of Autonomous Underwater*, 1–11. https://doi.org/doi:10.1201/9780203522301.ch3

**Eriksen, C. C., Osse, T. J., Light, R. D., Wen, T., Lehman, T. W., Sabin, P. L., … Chiodi, A. M.** (2001). Seaglider: A long-range autonomous underwater vehicle for oceanographic research. *IEEE Journal of Oceanic Engineering*, *26*(4), 424–436. https://doi.org/10.1109/48.972073

**Exocetus Autonomous Systems.** (n.d.). Coastal glider. [PDF file]. Rerieved from http://auvac.org/uploads/platform_pdf/Exocetus%20Coastal%20Glider%20new.pdf

**F. Myring, D.** (1981). A Theoretical Study of the Effects of Body Shape and Mach Number on the Drag of Bodies of Revolution in Subcritical Axisymmetric Flow, 36.

**Gao, T., Wang, Y., Pang, Y., & Cao, J.** (2016). Hull shape optimization for autonomous underwater vehicles using CFD. *ENGINEERING*

*APPLICATIONS OF COMPUTATIONAL FLUID MECHANICS*, *10*(1), 599–607. https://doi.org/10.1080/19942060.2016.1224735

**Graver, J.** (2005). Underwater gliders: Dynamics, control and design (Doctoral dissertation, Princeton University). Retrieved from https://www.princeton.edu/~naomi/theses/jggraver-thesis-4-11-05.pdf

**Hajivand, A., Mousavizadegan, S., Sadeghian, M., & Fadavi, M.** (2016). Effect of hydroplane profile on hydrodynamic coefficients of an autonomous underwater vehicle, *67*, 19–41.

**hang Hou, Y., Liang, X., & yang Mu, X.** (2018). AUV hull lines optimization with uncertainty parameters based on six sigma reliability design. *International Journal of Naval Architecture and Ocean Engineering*, *10*(4), 499–507. https://doi.org/https://doi.org/10.1016/j.ijnaoe.2017.10.001

**Harada, C.** (2010). Ocean Gliders: A Technological Revolution for Oceanography. Retrieved October 20, 2018 from https://sites.google.com/a/opensailing.net/protei/news/oceanglidersatechnologicalrevolutionforoceanography

**Hızarcı, T.** (2015). Buoyancy Driven Underwater Glider. Undergraduate. İstanbul Technical University.

**Hızarcı. T.** (2018, September 9). Personal interview.

**Ichihashi, N., Ikebuchi, T., & Arima, M.** (2008). Development of an Underwater Glider with Independently Controllable Main Wings. *Proceedings of the Eighteenth*, 156–161. https://doi.org/10.1109/OCEANSKOBE.2008.4531062

**Kawaguchi, K., Tomoda, Y., Kobayashi, H., & Ura, T.** (1993). Development and sea trials of a shuttle type AUV" ALBAC". In *INTERNATIONAL SYMPOSIUM ON UNMANNED UNTETHERED SUBMERSIBLE TECHNOLOGY*.

**Kongsberg Maritime.** (n.d.). Underwater altimeter. Retrieved from https://www.km.kongsberg.com/ks/web/nokbg0240.nsf/AllWeb/188AD958095B7127C1256CFC00300A95?OpenDocument

**Kongsberg Underwater Technology.** (2013). Seaglider. Retrieved from http://auvac.org/uploads/platform_pdf/Seaglider_product_specification.pdf

**Kostaschuk, R., Best, J., Villard, P., Peakall, J., & Franklin, M.** (2005). Measuring flow velocity and sediment transport with an acoustic Doppler current profiler. *Geomorphology*. https://doi.org/10.1016/j.geomorph.2004.07.012

**Liu, H.-L., & T. Huang, T.** (1998). Summary of DARPA Suboff Experimental Program Data, 28.

**Liu, Yanji & Ma, Jie & Ma, Ning & Huang, Zhijian.** (2018). Experimental and Numerical Study on Hydrodynamic Performance of an Underwater Glider. Mathematical Problems in Engineering. 2018. 1-13. 10.1155/2018/8474389.

**OpenFOAM Foundation.** (n.d.). OpenFOAM and The OpenFOAM Foundation. Retrieved from https://openfoam.org/

**Rudnick, D. L., Davis, R. E., Eriksen, C. C., Fratantoni, D. M., & Perry, M. J.** (2004). Underwater gliders for ocean research. Marine Technology Society Journal, 38(2), 73-84.

**Sezen, S., Dogrul, A., Delen, C., & Bal, S.** (2018). Investigation of self-propulsion of DARPA Suboff by RANS method. *Ocean Engineering*, *150*, 258–271. https://doi.org/https://doi.org/10.1016/j.oceaneng.2017.12.051

**Shapiro, J.** (2017). PLOCAN Glider School 2017. Speech, Oceanic Platform of the Canary Islands.

**Singh, Y., Bhattacharyya, S., & Idichandy, V.** (2017). CFD Approach to Modelling, Hydrodynamic Analysis and Motion Characteristics of a Laboratory Underwater Glider with Experimental Results. *Journal of Ocean Engineering and Science*. https://doi.org/10.1016/j.joes.2017.03.003

**Szondy, D.** (2015). Europe's first ultra-deep-sea robotic glider to monitor deep sea pollution. Retrieved from https://newatlas.com/bridges-ultra-deep-sea-robotic-glider/38336/

**Teledyne Marine.** (n.d.). Slocum G3 Glider. Retrieved from http://www.teledynemarine.com/slocum-glider/

**The Next Frontier in Ocean Exploration.** (n.d.). Retrieved from https://www.ocean.washington.edu/story/Deepgliders

**Tips and tricks in OpenFOAM.** Presentation. Retrieved from http://www.wolfdynamics.com/wiki/OFtipsandtricks.pdf

**Underwater Glider Platform.** (n.d.). [PDF file]. Retrieved from http://auvac.org/uploads/configuration_spec_sheets/USM-Robotics%20UW%20Glider.pdf

**Wang, Z., Li, Y., Wang, A., & Wang, X.** (2015). Flying wing underwater glider: Design, analysis, and performance prediction. In *International Conference on Control, Automation and Robotics*, *ICCAR 2015* (pp. 74–77). https://doi.org/10.1109/ICCAR.2015.7166005

**WHOI Underwater Glider Operations.** (n.d.). Retrieved from http://gliders.whoi.edu/instrumentation/

**Williams, A.** (n.d.). OSUG: Open-source underwater glider. Retrieved from https://hackaday.io/project/20458-osug-open-source-underwater-glider

**Yu, P., Wang, T., Zhou, H., & Shen, C.** (2018). Dynamic modeling and three-dimensional motion simulation of a disk type underwater glider. *International Journal of Naval Architecture and Ocean Engineering*. https://doi.org/10.1016/j.ijnaoe.2017.08.002

**CURRICULUM VITAE**

**Name Surname** : Mehmet Ozan ŞERİFOĞLU

**Place and Date of Birth** : 13/03/1992 - İstanbul

**E-Mail** : ozanserifoglu@gmail.com

**EDUCATION**

- **B.Sc.:** 2015 - Istanbul Technical University, Department of Shipbuilding and Ocean Engineering

**PROFESSIONAL EXPERIENCE AND REWARDS**

- 2017 – Co-founder of Narval R&D
- 2017 - Research Assistant at Istanbul Technical University, Faculty of Naval Architecture and Ocean Engineering